Dynamic regulation of B cell complement signaling is integral to germinal center responses

Arun Cumpelik[1,2], David Heja[1,2,8], Yuan Hu[1,2], Gabriele Varano[3,9], Farideh Ordikhani[1,2,4], Mark P. Roberto[3,5], Zhengxiang He[6], Dirk Homann[6], Sergio A. Lira[6], David Dominguez-Sola[3,4,6,7,10] ✉ and Peter S. Heeger[1,2,6,10] ✉

Maturation of B cells within germinal centers (GCs) generates diversified B cell pools and high-affinity B cell antigen receptors (BCRs) for pathogen clearance. Increased receptor affinity is achieved by iterative cycles of T cell–dependent, affinity-based B cell positive selection and clonal expansion by mechanisms hitherto incompletely understood. Here we found that, as part of a physiologic program, GC B cells repressed expression of decay-accelerating factor (DAF/CD55) and other complement C3 convertase regulators via BCL6, but increased the expression of C5b-9 inhibitor CD59. These changes permitted C3 cleavage on GC B cell surfaces without the formation of membrane attack complex and activated C3a- and C5a-receptor signals required for positive selection. Genetic disruption of this pathway in antigen-activated B cells by conditional transgenic DAF overexpression or deletion of C3a and C5a receptors limited the activation of mechanistic target of rapamycin (mTOR) in response to BCR–CD40 signaling, causing premature GC collapse and impaired affinity maturation. These results reveal that coordinated shifts in complement regulation within the GC provide crucial signals underlying GC B cell positive selection.

Effective humoral responses to exogenous pathogens or vaccines depend on the generation of high-affinity antibodies by affinity maturation. This key process is accomplished in GCs, specialized compartments within secondary lymphoid organs[1,2] where B cells undergo iterative cycles of immunoglobulin gene somatic hypermutation, affinity-driven positive selection and clonal expansion[2]. Positive selection is triggered by enhanced B cell access to costimulatory signals from recruited follicular helper T cells (T$_{FH}$) following antigen capture and presentation[2–4]. These signals determine the fate of GC B cells (survival and proliferation versus cell death or differentiation), and are critical for sustaining the GC reaction and its immunological outputs[2,5].

The precise molecular signals that drive positive selection and promote survival/expansion of selected GC B cells remain incompletely understood[2]. Previous studies showed that positive selection involves activation of PI3K–AKT and mTOR signaling, as well as MYC expression[2,3,6,7]. While synergistic activation of CD40 and the BCR initiates triggering of a subset of these signals[4], integration of additional, unidentified 'help' cues is thought to actively contribute to successful selection[2]. Building upon previous work linking complement activation to adaptive T cell responses[8–11] and the observation that GC B cells specifically lack surface expression of the complement regulator DAF/CD55, we decided to investigate the notion that complement-initiated signaling impacts GC fate and function.

Decay-accelerating factor is a glycophosphatidylinositol-(GPI)-anchored, complement system regulator that functions only on DAF-expressing cell surfaces[12]. DAF accelerates the decay of multimeric C3 convertases, limiting amplification/progression of the complement cascade and preventing formation of the C3- and C5-cleavage products C3a and C5a, respectively[12]. It is encoded within the regulators of complement activation (RCA) syntenic region of human chromosome 1, which includes $Cr1$ (CD35), $Cr2$ (CD21), C4b-binding protein ($C4BP$) and human membrane cofactor protein ($MCP/Cd46$)[13]. In mice, chromosome 1 encodes a differently arranged but syntenic region for homologs of $DAF/Cd55$, $Cr2$, $C4bp$ and $Cr1l$ ($Crry$, absent in humans)[14]. These regulators collectively dissociate C3 convertases and/or facilitate inactivation of C3b to iC3b. Herein we demonstrate that reprogramming of surface complement regulator expression in GC B cells by BCL6 enables local C3a/C5a-receptor signaling and optimal mTOR activation required for positive selection and GC homeostasis.

Results

Coordinated shifts in complement regulators on GC B cells. We initially observed that DAF is highly expressed on IgD⁺ B cells, but undetectable on GL7⁺ B cells, in the spleen of 4-hydroxy-3-nitrophenyl-acetyl-keyhole-limpet hemocyanin (NP-KLH)-immunized mice (Fig. 1a). Flow cytometric analyses confirmed high DAF surface expression on naive murine (B220⁺IgD⁺) and human (CD19⁺IgD⁺CD38^{lo}) B cells (Fig. 1b,c and Extended Data Fig. 1a,b). DAF expression on murine IgD⁻ GC B cells, defined by the expression of markers GL7 and Fas, and on human IgD⁻ GC B cells, defined by the expression of surface markers CD38 and CD10, is >tenfold lower compared to naive B cells. DAF expression recovers in murine (IgD⁻GL7⁻Fas⁻CD38⁺) and human memory

[1]Renal Division, Department of Medicine, Icahn School of Medicine at Mount Sinai, New York, NY, USA. [2]Translational Transplant Research Center, Icahn School of Medicine at Mount Sinai, New York, NY, USA. [3]Department of Oncological Sciences, Icahn School of Medicine at Mount Sinai, New York, NY, USA. [4]Tisch Cancer Institute, Icahn School of Medicine at Mount Sinai, New York, NY, USA. [5]Graduate School of Biomedical Sciences, Icahn School of Medicine at Mount Sinai, New York, NY, USA. [6]Precision Immunology Institute, Icahn School of Medicine at Mount Sinai, New York, NY, USA. [7]Department of Pathology, Icahn School of Medicine at Mount Sinai, New York, NY, USA. [8]Present address: eGenesis Inc., Cambridge, MA, USA. [9]Present address: Department of Translational Medicine, Laboratory for Advanced Therapy Technologies, University of Ferrara, Ferrara, Italy. [10]These authors jointly supervised this work: D. Dominguez-Sola and P. S. Heeger. ✉e-mail: david.dominguez-sola@mssm.edu; peter.heeger@mssm.edu

(CD19^{+}IgD^{-}CD27^{+}) B cells. In immunized mice, DAF downregulation on GC B cells was evident by day 6 after immunization (mean fluorescence intensity (MFI) = 5,030 ± 300.2, $n = 4$), decreased further on day 8 (MFI = 1,753 ± 26.66, $n = 4$; $P < 0.001$ versus day 6, unpaired t-test) to a minimum level on day 10 (MFI = 560.5 ± 63.58, $n = 4$; $P < 0.001$ versus days 6 and 8, unpaired t-test) and was maintained through to day 12 (MFI = 516.8 ± 65.22, $n = 4$; not significant versus day 10, unpaired t-test). DAF downregulation was commensurate in light-zone (CD86^{hi}CXCR4^{lo}), dark-zone (CD86^{lo}CXCR4^{hi}) and gray-zone[15] (CD86^{hi}CXCR4^{hi}) GC B cells (Extended Data Fig. 1c). Analysis of other RCA proteins showed lower CR1/2 on murine GC B cells and very low to absent *Crry* expression in all B cell subsets (Fig. 1b and Extended Data Fig. 1d). Human GC B cells also expressed consistently lower levels of CD46, CR1 and CR2 (Fig. 1c and Extended Data Fig. 1e). We observed, reciprocal changes in messenger RNA expression of human and syntenic murine RCA genes in GC and naive B cells (Fig. 1d,e and Extended Data Fig. 1f). In contrast to RCA members, murine and human GC B cells expressed higher levels of the membrane attack complex (MAC) inhibitor CD59 (protectin, encoded outside the RCA; Fig. 1b,c and Extended Data Fig. 1d,e). Both murine and human GC B cells stained positive for the C3 cleavage product C3b (Fig. 1f and Extended Data Fig. 1g), and GCs in human tonsil tissue sections stained positive for C3b, C4b and C6 but not C9 (Fig. 1g and Extended Data Fig. 1h), reflecting the functional absence of C3 convertase regulation but the presence of CD59 activity. Together, these results demonstrate that the coordinated and dynamic reorganization of complement regulatory proteins facilitates C3 convertase activity on GC B cells while blocking MAC formation (Extended Data Fig. 2a).

BCL6 represses DAF expression in GC B cells. The transcription factor BCL6 is required for GC B cell generation and is expressed in committed GL7^{+}CCR6^{+}CD38^{+} B cells[5] before GC entry (days 3–4 post immunization)[16,17]. To further delineate the kinetics of DAF downregulation in GC B cells, we immunized BCL6-YFP reporter mice[17] and, 3 days later, analyzed DAF and BCL6 protein expression (BCL6-YFP) on IgD[-]GL7^{+} B cells (Fig. 2a and Extended Data Fig. 2b). These analyses showed that, on day 3 (before GC formation/coalescence), BCL6-YFP^{+} B cells were already lacking DAF expression, coinciding with the upregulation of BCL6 expression during early GC commitment.

Analysis of available gene expression data on human GC-derived B cell lymphoma and multiple myeloma cell lines confirmed the inverse correlation of *DAF* and *BCL6* expression (Extended Data Fig. 2c). BCL6 is a major transcriptional repressor in GC B cells[16] and, based on available human GC B cell chromatin immunoprecipitation sequencing (ChIP–seq) data[18], it is enriched at an active 5′ proximal regulatory region and an intronic enhancer in the *CD55* gene (defined by the distribution of H3K4me1 and H3K4me3 histone marks; Fig. 2b), suggesting that BCL6 can directly modulate DAF expression. We further noted BCL6 enrichment at multiple regulatory regions throughout the RCA (including 5′ regulatory regions of *CD21*, *CR1/2* and *C4bBP-CD46*), but this was notably

absent from regulatory regions upstream of *CD59* (Extended Data Fig. 2d,e). Consistent with these observations, transient BCL6 overexpression in KMS27 cells (multiple myeloma cell line, BCL6^{-}DAF[+]) reduced surface DAF and CD46 expression without altering CD59 expression (Fig. 2c,d). Conversely, overexpression of a dominant negative BCL6 mutant[19] (BCL6-ZF; Fig. 2e,f) in SUDHL5 B cell lymphoma cells (BCL6^{hi}DAF[lo]) increased surface DAF and CD46 expression without altering CD59. Similarly, BCL6 inactivation by a small-molecule BCL6 inhibitor[20] (FX1) increased DAF (5/5 lymphoma lines tested) and CD46 expression (2/4 lines increased, 2/4 no change; Fig. 2g,h). CD59 expression was also increased under these conditions (Fig. 2i; 3/3 lines tested). Finally, transient BCL6 overexpression in TOLEDO B cells (B cell lymphoma, BCL6^{lo}DAF[hi]), but not of two truncated, transcriptionally inactive BCL6 variants[19], repressed luciferase reporter activity driven by the two regulatory regions identified in the *CD55* gene (Fig. 2j). Thus, BCL6 is a direct transcriptional repressor of *DAF* gene expression in GC B cells.

GC homeostasis requires C3aR1–C5aR1 signaling in GC B cells. To investigate the functional relevance of DAF downregulation in GC B cells, we engineered mice expressing a conditional (Cre-lox), transmembrane-domain-containing, transgenic form of DAF (DAF-TM; Extended Data Fig. 3a) and intercrossed these mice with B cell-specific *CD19*-Cre[21] or *Cγ1*-Cre mice[22]. While *CD19*-Cre is active throughout B cell development[21], *Cγ1*-Cre-mediated recombination is restricted to GL7^{hi}Fas[hi] GC B cells soon after immunization (25–50% at day 4) and is maximal (75–90%) at the peak of the GC reaction[22] (days 10–14). Using B cells isolated from *DAF-TM^{+/+} × CD19*-Cre^{+/-} mice, we confirmed expression of a noncleavable DAF-TM protein on GC B cell surfaces that functionally limits C3b deposition (Extended Data Fig. 3b–d). Control analyses showed that GPI-anchored CD59 is cleaved from the same GC B cells (Extended Data Fig. 3e,f). Consistent with published kinetics of *Cγ1*-Cre activity[22], sequential analyses of GL7^{+}Fas[+] GC B cells from immunized *DAF-TM^{+/+} × Cγ1*-Cre^{+/-} (DAF-TM[Cγ1]) mice showed expression of noncleavable, functional DAF-TM protein as early as day 4 (~30% of GC B cells), peaking by day 10 post immunization with NP-KLH (>90% of GC B cells; Extended Data Fig. 4a). We also observed detectable DAF-TM expression on ~10% of activated GL7^{+}CCR6^{+}CD38^{+} B cells[5] on day 4, increasing to 75% by day 10 (Extended Data Fig. 4a). On days 10–12 we observed two- to threefold higher DAF expression on DAF-TM[Cγ1] GC B cells versus Cre^{+/-} controls (Fig. 3a), without alterations in expression levels of CD59, CR1/2 or *Crry* among naive, GC and memory B cells (Extended Data Fig. 4b–d).

Flow cytometry analyses of DAF-TM[Cγ1] mice immunized with NP-KLH (Fig. 3b–e) and sheep red blood cells (SRBC; Extended Data Fig. 4e–g) showed lower relative and absolute frequencies of splenic GC B cells (~threefold; $P < 0.001$). GCs induced following NP-KLH (Fig. 3d,e) and SRBC immunization (Extended Data Fig. 4g) initially formed (days 4–8) and adequately polarized (Extended Data Fig. 4h), but did not continue to expand beyond days 8–10 (coinciding with the peak of DAF-TM transgene expression).

Fig. 1 | GC B cells downregulate expression of DAF (CD55) and other C3/C4 convertase inhibitors within the RCA. a, Representative (ten different experiments) immunofluorescence analysis of a splenic GC from a WT C57BL/6 mouse, 10 days post immunization with NP-KLH, stained for IgD (naive B cells), GL7 (GC B cells (GCB)) and DAF. Scale bars, 50 μm. **b,c**, Flow cytometry analysis of mouse (**b**) and human (**c**) B cell subsets stained for DAF, CR1/2, Crry (mouse), CD46 (human) and CD59, as indicated. Each dot represents one biological replicate. Gating strategy is shown in Extended Data Fig. 1a,b. **d**, DAF mRNA expression in murine B cell subsets. Data extracted from the Immgen database[56]. PC, plasma cells. **e**, Heatmap (top, microarray) and transcript number (bottom, RNA-seq; inset numbers denote fold change) of human complement regulator expression; data sources: GSE2350 (heatmap) and GSE139833 (bar graph). **f**, Flow cytometry analysis of mouse (left) and human (right) B cell subsets stained for C3b. Each dot represents one biological replicate. **g**, Representative immunofluorescence analysis of human tonsil GC staining for C3b, C4d and C6 but not C9 (positive control shown in Extended Data Fig. 1h). Scale bars, 50 μm. **a,g**, Representative of more than three experiments. Data are presented as MFI ± s.e.m.; *$P < 0.05$, **$P < 0.01$, ***$P < 0.001$, ****$P < 0.0001$ by either one-way analysis of variance (ANOVA) with Bonferroni post-test (**b,c,f**) or mean ± s.e.m. and Student's t-test (**e**, bottom). Bmem, memory B cells; NS, not significant; AU, arbitrary units.

NP-KLH-induced GCs had prematurely collapsed by day 12 (Fig. 3d,e), associated with reduced numbers of memory and plasma cells (Fig. 3f and Extended Data Fig. 4i–k), together demonstrating disruption of GC function/maintenance.

The absence of DAF expression on GC B cells would be expected to lift restraint on cell surface C3 convertase formation, resulting in augmented release of C3a and C5a anaphylatoxins[8,9,23] (Extended Data Fig. 2a) and subsequent signaling through their respective
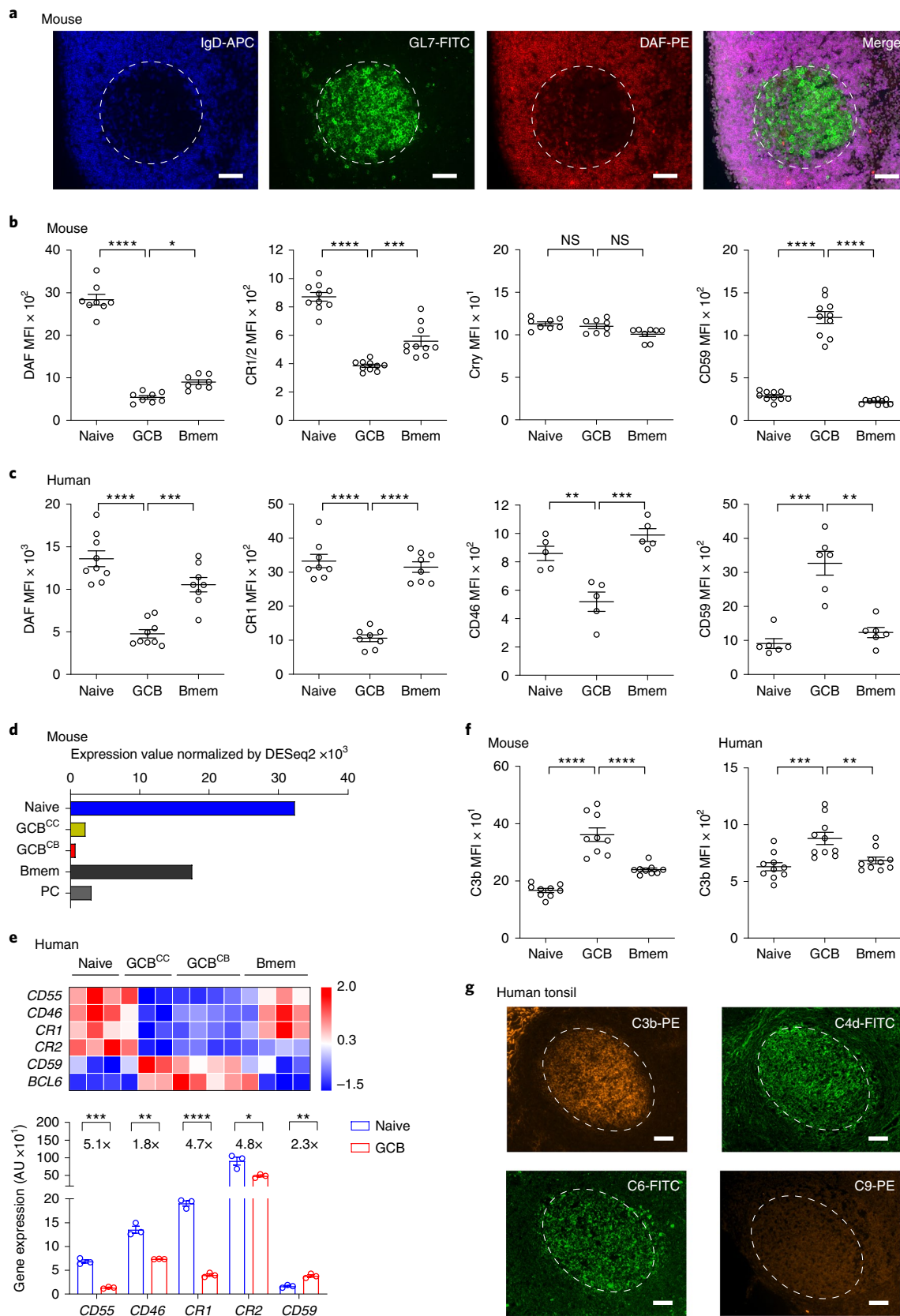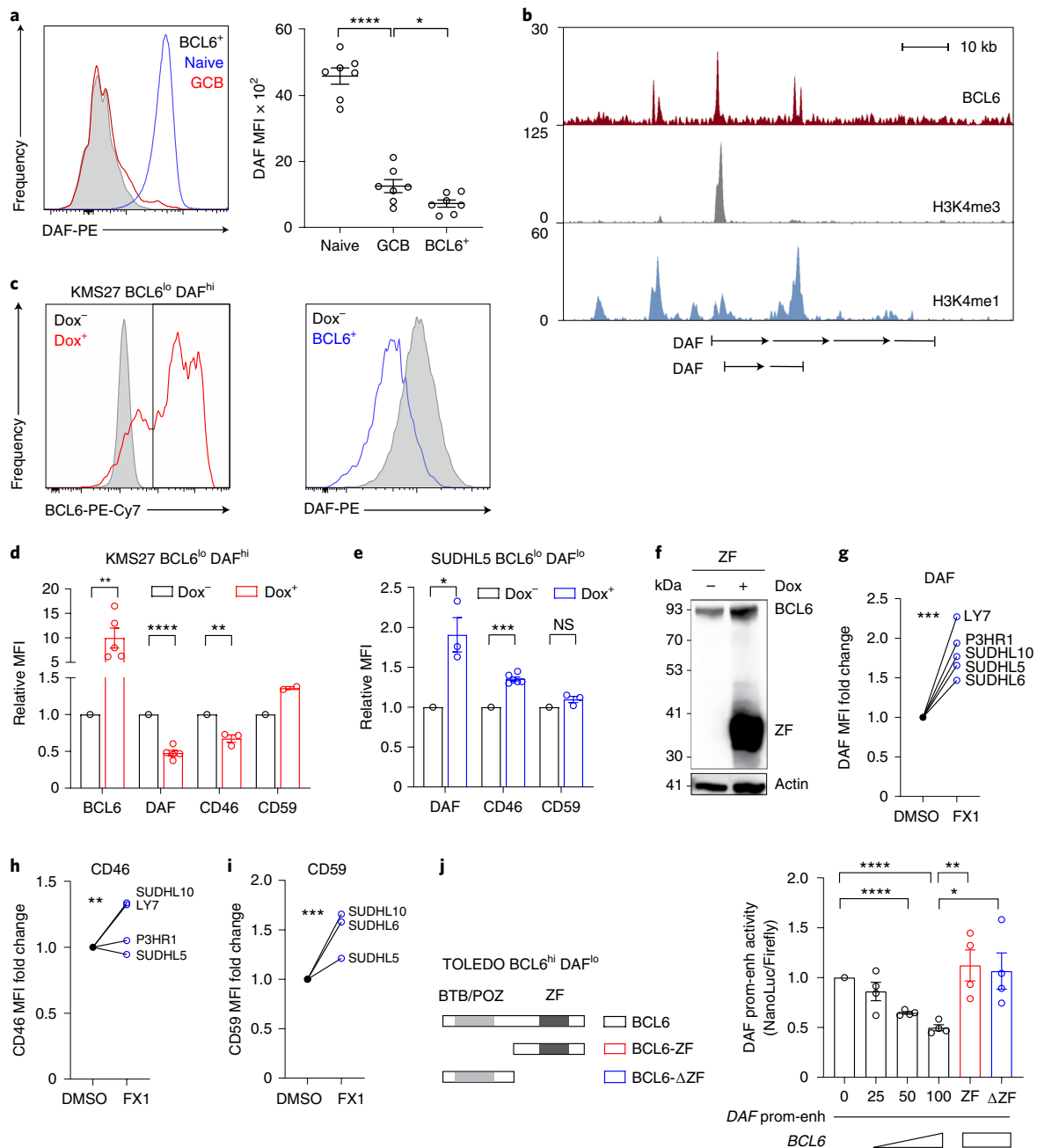
Fig. 2 | BCL6 transcriptionally represses DAF expression in GC B cells. a, Representative histogram (left) and quantified results (right) of DAF (CD55) and BCL6 expression in BCL6-YFP+ B cells, day 3 post immunization (gating strategy shown in Extended Data Fig. 2b); mean ± s.e.m. **b**, ChIP–seq analysis of human GCB cells (tonsil) showing distribution of BCL6, H3K4me1 and H3K4me3 marks at the *CD55* gene (from GSE68349 and GSE67494)[18,57]. **c,d**, Representative histograms for BCL6 (**c**, left) and DAF (**c**, right) with quantification (**d**) for BCL6, DAF, CD46 and CD59 on KMS27 (multiple myeloma) cells following BCL6 overexpression (*n* = 5 for BCL6 and DAF, *n* = 3 for CD46, *n* = 2 for CD59). **e,f**, Quantified changes in expression of DAF, CD46 and CD59 in SUDHL5 DLBCL B-lymphoma cells (**e**) (DAF and CD59, *n* = 3; CD46, *n* = 6) following transfection with a dominant negative (ZF) BCL6 (**f**, representative immunoblot). Anti-BCL6 antibody recognized a region present in the ZF domain of this protein (BCL6, full-length protein). **g–i**, Fold change in surface expression of DAF (**g**), CD46 (**h**) and CD59 (**i**) by flow cytometry 24 h after the addition of either BCL6 inhibitor FX1 (50 mM) or DMSO control. FX1 significantly upregulated DAF in five cell lines (SUDHL5, *n* = 6; SUDHL6, *n* = 4; SUDHL10, *n* = 8; P3HR1, *n* = 2; OCI-LY7, *n* = 3). *P* value is a summary of all replicates for all lines. FX1 upregulated CD46 in OCI-LY7 (*n* = 1) and SUDHL10 (*n* = 2) (*P* value shown for these three combined replicates), with no effect in either SUDHL5 (*n* = 2) or P3HR1 (*n* = 2) (*P* value for these combined replicates not significant). FX1 upregulated CD59 in 3/3 lines (SUDHL5, *n* = 3; SUDHL6, *n* = 4; SUDHL10, *n* = 3). The *P* value is shown for these ten combined replicates from the three cell lines. Data are presented as normalized to DMSO levels for each experiment. **j**, Left: construct schematics for BCL6, BCL6 DNA binding domain ZF and BCL6 lacking DNA binding domain delta-ZF. BTB/POZ, protein–protein interaction domain. Right: quantified luciferase signal under each condition. **a–j**, Data are presented as mean ± s.e.m.; *P < 0.05, **P < 0.01, ***P < 0.001, ****P < 0.0001 by ANOVA with either Bonferroni post-test (**a**,**j**), two-tailed unpaired *t*-test (**a**,**d**,**e**) or two-tailed paired *t*-test (**g**).
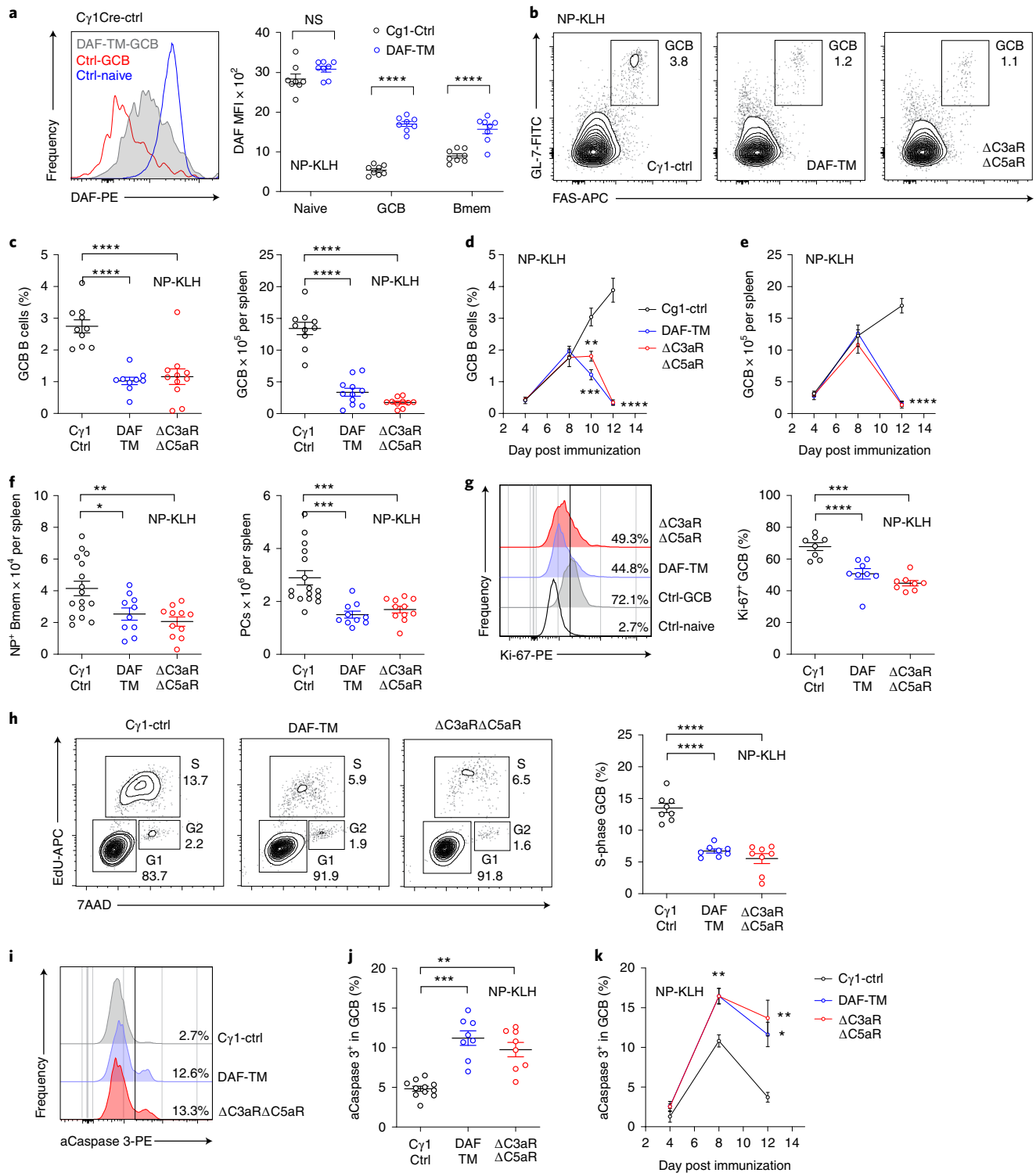
Fig. 3 | Transgenic DAF overexpression or absence of C3ar1–C5ar1 on GC B cells aborts GC formation. a, Representative histogram (left) and quantitation (right) of DAF (CD55) expression on GCB subsets from DAF-TM$^{C\gamma1}$ (blue) and $C\gamma1$-Cre$^{+/-}$ (control (Ctrl), black) mice at day 12 post immunization with NP-KLH. **b–k**, All experiments and analyses were performed on groups of day 10–12, NP-KLH-immunized, DAF-TM$^{C\gamma1}$ (DAF-TM), $\Delta C3ar1/C5ar1^{C\gamma1}$ (ΔC3aR/ΔC5aR) and control $C\gamma1$-Cre$^{+/-}$ (Cγ1-Ctrl) mice. **b,c**, Representative contour plots (**b**) and quantification (**c**) of day 12 percentage (left) and total (right) splenic GC B cells. **d,e**, Kinetic analysis of relative percentages (**d**) and total splenic GC B cells (**e**). **f**, Quantification of day 12 splenic Bmem (left, B220$^+$IgD$^-$GL7$^-$Fas$^-$CD38$^+$NP$^+$) and plasma cells (right, CD19$^+$B220^{dim}CD138$^+$ PCs) (Extended Data Fig. 4i–k). **g**, Representative histograms (left) and quantification of percentage of Ki67$^+$ GC B cells (right). **h**, Representative contour plots (left) and quantitation (right) of EdU incorporation and DNA content (7-aminoactinomycin D (7AAD)) in GC B cells. S, synthesis phase; G, growth phase. **i–k**, Representative histograms (**i**), d12 quantification (**j**) and kinetics (**k**, $n = 4$ per time point for each genotype) of activated caspase 3$^+$ (aCaspase 3) in splenic GC B cells. Data are presented as mean values $\pm$s.e.m.; *$P < 0.05$, **$P < 0.01$, ***$P < 0.001$, ****$P < 0.0001$ by ANOVA with Bonferroni post-test. For kinetics in **d,e,k**, three genotypes were compared at each time point. Each dot represents one biological replicate.
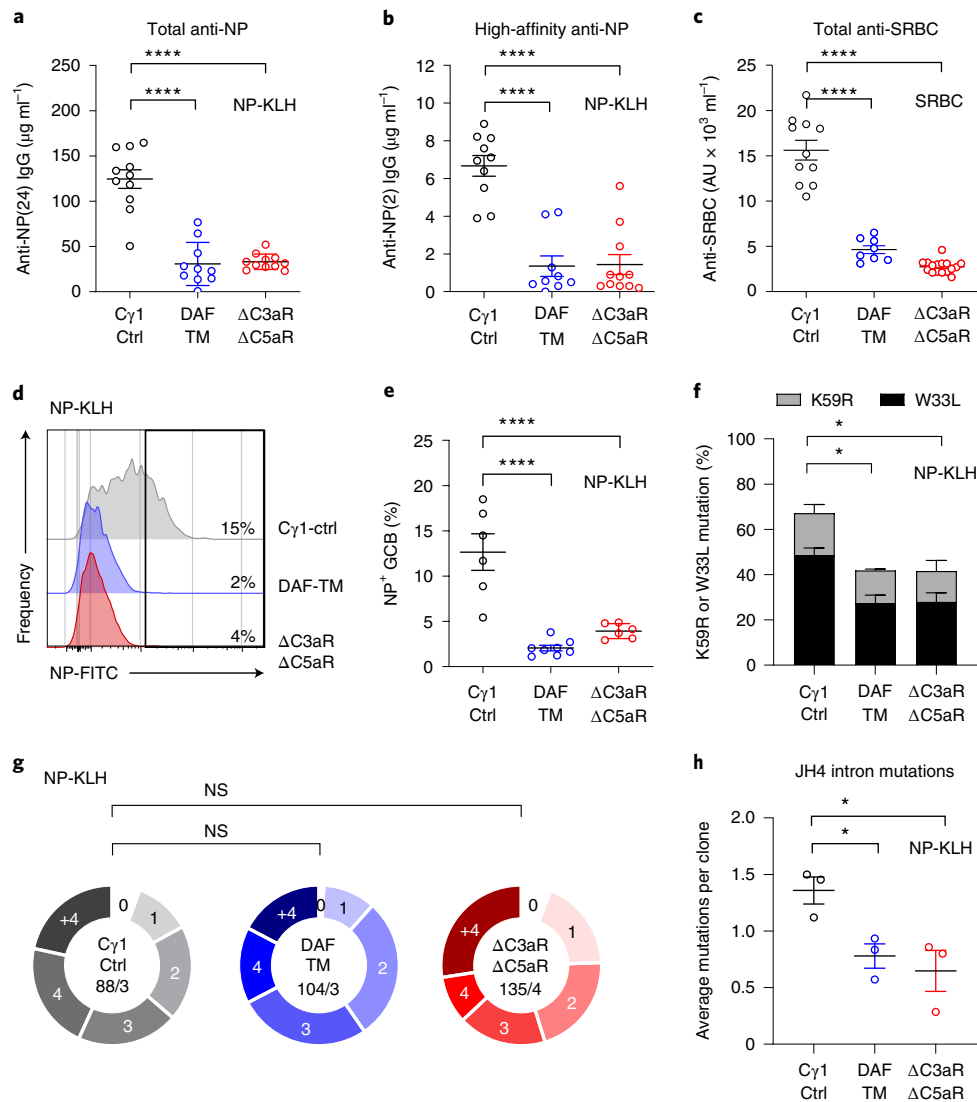
Fig. 4 | Transgenic DAF overexpression or absence of C3ar1–C5ar1 in GC B cells limits affinity maturation. a,b, Serum ELISA assay for total anti-NP(24) (**a**) and high-affinity anti-NP(2) (**b**) antibodies from day 12 immunized mice. **c**, Quantified serum anti-SRBC antibodies from day 12 SRBC-immunized DAF TM, ΔC3aRΔC5aR and control Cγ1 Ctrl mice. **d,e,** Representative flow histogram (**d**) and quantification (**e**) of day 12 splenic NP-specific GCB cells from DAF-TM^{Cγ1}, Δ*C3ar1/C5ar1*^{Cγ1} and *Cγ1*-Cre$^{+/-}$ mice. **f,g,** Quantified frequencies of high-affinity W33L$^+$ (±K59R or K59R alone) λ BCRs (**f**) with clone distribution (**g**) based on the number of somatic mutations (0 to >4). The numbers of clones and animals analyzed per genotype are indicated in the center of each circle. **h**. Quantification of mutation frequency per 100 bp in JH4 segments, plotted by genotype (n = 3 animals per group). Data are presented as mean values ± s.e.m. *$P < 0.05$, ****$P < 0.0001$ by ANOVA with Bonferroni post-test (**a–c,e,h**), Fisher's exact test (**f**) or chi-square (**g**). Each dot represents one biological replicate (Supplementary Table 1).

receptors. These receptors (C3aR1 and C5aR1) were upregulated on murine and human GC B cells (Extended Data Fig. 5a–d), along with C5aR2–C5L2, an alternative 'decoy' receptor for C5a[24] (Extended Data Fig. 5e). Indeed, GC responses in newly generated *C3ar1*$^{fl/fl}$*C5ar1*$^{fl/fl}$ × *Cγ1*-Cre$^{+/-}$ mice (Δ*C3ar1/C5ar1*^{Cγ1}), in which C3aR1/C5aR1 are absent on GC B cells, phenocopied those of DAF-TM^{Cγ1} mice (Fig. 3b–f and Extended Data Figs. 4e–g), including reduced GC size on day 10 (Extended Data Fig. 5f–g). Absence of either C3aR1 or C5aR1 showed an intermediate phenotype (Extended Data Fig. 4e,f). These defects in GC formation and maintenance in Δ*C3ar1/C5ar1*^{Cγ1} and DAF-TM^{Cγ1} mice were associated with substantial reductions in the fraction of actively proliferating cells (Ki67 staining and 5-ethynyl-2'-deoxyuridine (EdU) incorporation; Fig. 3g,h) and with significant increases in the percentage of active caspase 3 positivity (a bona fide marker of cell death in GCs[25];

Fig. 3i–k). All these parameters indicate severe disruption of GC homeostasis.

We also analyzed GCs in mice with germline deficiencies in various complement components and in C3$^{-/-}$–wild-type (WT) bone marrow chimeras. Compared to Δ*C3ar1/C5ar1*^{Cγ1} mice, CD21 (CR2) deficiency only modestly reduced GC formation in the setting of high antigen availability, consistent with previous observations[2,26,27] (Extended Data Fig. 6a,b). Optimal GC formation required systemic C3 as well as C1q, but not factor B or mannose-binding lectin (MBL), the latter implicating the classical pathway of complement activation (Extended Data Fig. 6c).

The disruption of GC responses in DAF-TM^{Cγ1} and Δ*C3ar1/C5ar1*^{Cγ1} mice was also associated with a pronounced defect in antibody generation, with four- to sixfold lower titers of total and high-affinity anti-NP antibodies in NP-KLH-immunized

mice ($P < 0.001$; Fig. 4a,b) and similarly reduced titers of anti-SRBC (Fig. 4c) antibodies in SRBC-immunized mice. Together with the observed fourfold fewer NP-reactive GC B cells ($P < 0.01$; Fig. 4d,e), the data suggested impaired affinity maturation. We thus quantified frequencies of BCR somatic mutations known to confer high affinity, sequencing the variable regions of the λ^+ BCRs in GC B cells of DAF-TM[Cγ1], $\Delta C3ar1/C5ar1$[Cγ1] and control mice immunized with NP-KLH (Fig. 4f,g and Supplementary Table 1). DAF-TM[Cγ1], $\Delta C3ar1/C5ar1$[Cγ1] GC B cells carried ~twofold fewer high-affinity (W33L, K59R) BCR mutations in Vh186.2 immunoglobulin regions. Analysis of intronic sequences downstream of the JH4 gene, a region targeted by somatic hypermutation activity but not subject to selection[28], showed that DAF-TM[Cγ1] and $\Delta C3ar1/C5ar1$[Cγ1] GC B cells had an overall lower frequency of somatic hypermutation (Fig. 4h and Supplementary Table 1), implying that the reduction in affinity maturation in these mice is due to reduced cycling and hypermutation of these cells within GCs.

Competitive selection of GC B cells requires C3aR1–C5aR1. To gain further mechanistic insights into these defects, we performed RNA-sequencing (RNA-seq) on flow-sorted GL7$^+$Fas$^+$ B cells at day 10 after SRBC immunization (at the peak of DAF-TM expression and GC size plateau in DAF-TM mice; Fig. 3d,e and Extended Data Fig. 4g), sorting for DAF$^+$ GC B cells in DAF-TM[Cγ1] mice. Using supervised analysis, we identified ~85 differentially expressed genes between DAF-TM[Cγ1] and control GC B cells (DESeq2, adjusted $P < 0.05$ cutoff; Supplementary Table 2). Approximately two-thirds of these genes, including DAF, were upregulated in DAF-TM[Cγ1] GC B cells and belonged to families of membrane-associated proteins and/or secreted molecules involved in cell–cell interactions, cell adhesion and/or chemokine-driven cell motility (Extended Data Fig. 7a and Supplementary Table 2). Among genes downregulated, we found those encoding subunits of the PI3-K signaling complex (*Pik3cg*, *Pik3c2a*) and other proteins reportedly involved in the control of fatty acid and RNA metabolism (*Cdk19*, *Apobec1*, *Ptbp3*, *Insig1*, *Apoc2*) (Supplementary Table 2). A fraction of differentially expressed genes in DAF-TM[Cγ1] GC B cells encoded proteins involved in immunoregulatory interactions and chemokine signaling, with increased expression levels of *Ccr7*, *Ccl5*, *Ccl6*, *Tlr7*, *Sell* (*Cd62l*) and *S1pr1* (Fig. 5a,b). Activated GL7$^+$Fas$^+$ B cells at the interface between the B cell follicle and the T cell zone (B–T border), or CCR6$^+$CD38$^+$GL7$^+$Fas$^+$ pre-GC cells[5,29], express many of these factors, which are typically downregulated as activated B cells enter and expand in the GC (for example, *Ccr7*, *Tlr7*, *S1pr1*, *Sell/Cd62l*)[30–34]. Accordingly, gene set enrichment analysis (GSEA) detected enrichment for pre-GC gene signatures in DAF-TM[Cγ1] GC B cells (Fig. 5c). Flow cytometry analyses confirmed higher expression of

CCR7, TLR7, S1P1 and CD62L on GL7$^+$Fas$^+$ B cells in DAF-TM[Cγ1] and $\Delta C3ar1/C5ar1$[Cγ1] mice (Fig. 5d and Extended Data Fig. 7b,c). We also found increasing frequencies of CCR6$^+$CD38$^+$GL7$^+$Fas$^+$ B cells in DAF-TM[Cγ1] and $\Delta C3ar1/C5ar1$[Cγ1] mice at days 6–10 post immunization (Fig. 5e,f), suggesting the accumulation of B cells at transitional stages between naive and GC B cell phenotypes[5,29]. Immunofluorescence analysis of splenic tissue sections (Extended Data Fig. 5g) showed that GL7$^+$ cells were confined to GCs in both $\Delta C3ar1/C5ar1$[Cγ1] and control mice, and did not form clusters at the B–T border[35,36].

To better understand these findings, we cotransferred equal numbers of BCR transgenic CD45.1/2 B18^{hi}×Cγ1-Cre$^{+/-}$ and CD45.2 B18^{hi} DAF-TM[Cγ1] B cells into CD45.1 recipients. Adoptive transfer of congenic B1-8^{hi} transgenic B cells enabled specific and time-sequential, comparative analysis of cell fate between antigen-activated DAF-TM$^+$ and control B cells in response to NP immunization. These experiments showed that CD45.2 B18^{hi} DAF-TM[Cγ1] B cells failed to expand (Fig. 5g–i), both in the extra-follicular compartment and particularly within GCs, as evidenced by higher CD45.1/2 versus CD45.2 ratios and higher competitive indices[37] (two- to fourfold depletion, increasing from day 5 to day 9) (Fig. 5i). In nonimmunized mice, the ratios of CD45.1/.2 versus CD45.2 cells remained stable (1:1 post transfer). We also observed a progressively increasing percentage of GL7$^+$Fas$^+$ B cells coexpressing CCR6 and CD38 within DAF-TM$^+$ versus control B18^{hi} cells (Fig. 5j). Thus, DAF-TM B cells were initially activated in response to NP (confirmed by the upregulation of CCR6$^+$, CD62L$^+$, GL7$^+$ and Fas$^+$) and could be recruited to GCs, but they (abnormally) retained early activation markers and were progressively outcompeted by WT B cells in all compartments. Collectively these findings, and the alterations noted above in B cell proliferation and cell death, suggest that the absence of DAF and effective C3aR1–C5aR1 signaling are both essential for optimal B cell expansion and competitive fitness during T-dependent antigen responses.

C3aR1–C5aR1 activate mTOR and MYC in GC B cells. Germinal center entry and positive selection are driven by concurrent signals triggered by the BCR and ligand–receptor interactions offered by T$_{FH}$ cells[2]. Coactivation of BCR and CD40 signaling initiates key survival pathways (for example, mTOR and MYC) essential for positive selection in the light zone[3,4], and activates E2F-dependent B cell expansion in the dark zone[38]. Consistent with these concepts, pathway GSEA using a library of signatures defining general biological processes (HALLMARK and Gene Ontology categories[39]) revealed a loss of gene sets related to MYC, mTOR, CD40 and E2F signaling, cellular proliferation and biosynthesis in DAF-TM[Cγ1] GC B cells (Fig. 6a and Extended Data Fig. 8a). These results implied

Fig. 5 | Defective expansion, delayed maturation and reduced competitive competencies of DAF-TM[Cγ1] and $\Delta C3ar1/C5ar1$[Cγ1] B cells during GC responses. a, Heatmap depicting relative mRNA expression levels (row normalization) of selected genes in GCB subsets (source: ImmGen database). **b**, Relative mRNA expression of genes shown in **a** in GC B cells isolated from SRBC-immunized DAF-TM[Cγ1] and Cγ1-Cre$^{+/-}$ mice on day 10 (RNA-seq, TPM). P values estimated using DESeq2. **c**, Enrichment plot depicting gene set distribution of a pre-GC gene signature in DAF-TM[Cγ1] versus Cγ1-Cre$^{+/-}$ GC B cells (GSE12845_PRE_GC_VS_DARKZONE_GC_TONSIL_BCELL_UP). **d**, Quantified percentage of CD62L$^+$ GC B cells and surface expression levels of TLR7, CCR7 and S1P1 (MFI, as indicated) on day 10 SRBC-immunized GL7$^+$Fas$^+$ GC B cells from DAF-TM, $\Delta C3aR\Delta C5aR$ and control Cγ1 Ctrl mice (representative plots shown in Extended Data Fig. 7b). **e,f**, Representative contour plots (**e**, three left-most panels), relative frequency (**e**, right, day 10) and kinetics (**f**) of CCR6$^+$CD38$^+$-expressing GC B cells in SRBC-immunized DAF-TM[Cγ1], $\Delta C3ar1/C5ar1$[Cγ1] and Cγ1-Cre$^{+/-}$ mice. **g–i**, In vivo competition of control (CD45.1/2 or CD45.2) and DAF-TM$^+$ (CD45.2) B1-8^{hi} cells in NP-KLH-immunized CD45.1 hosts. **g**, Representative day 6 flow cytometry plots following cotransfer of CD45.2 control versus CD45.1/2 control B1-8^{hi} cells (left) and CD45.2 DAF-TM$^+$ versus CD45.1/2 control B1-8^{hi} cells (right). **h**, Kinetics of control versus DAF-TM$^+$ B1-8^{hi} cell expansion in NP-KLH-immunized hosts. **i**, Kinetic analysis of control versus DAF-TM$^+$ B1-8^{hi} GC B cell ratios (left) and normalized competitive competency indices (right) for CD45.1/2 control/CD45.2 DAF-TM$^+$ B1-8^{hi} cells (blue) and CD45.1/2 control/CD45.2 ctrl B1-8^{hi} cells (black) in NP-KLH-immunized hosts; CD45.1/2 control/CD45.2 control B1-8^{hi} cells in unimmunized hosts (red). **j**, Kinetics of ratios of percentage GL7$^+$CCR6$^+$CD38$^+$/GL7$^+$Fas$^+$ GC B1-8^{hi} cells to DAF-TM$^+$ (blue) and control B1-8^{hi} cells (black). Data are presented as mean ± s.e.m.; *$P < 0.05$, **$P < 0.01$, ***$P < 0.001$, ****$P < 0.0001$ by ANOVA with either Bonferroni post-test (**c–j**; for kinetics in **f–j**, three genotypes were compared at each time point) or unpaired Student's t-test (**b**). Each dot represents one biological replicate. Bmem, memory B cells. NES, normalized enrichment score; FDR, false discovery rate.

that C3 convertase activity and C3aR1–C5aR1 signaling are also necessary for effective GC B cell activation in response to BCR/CD40 signals.

To test this concept, we immunized groups of DAF-TM[Cγ1], Δ*C3ar1/C5ar1*[Cγ1] and control *Cγ1*-Cre^{+/−} mice and, 10 days later, analyzed MYC expression and mTOR activity (marked by
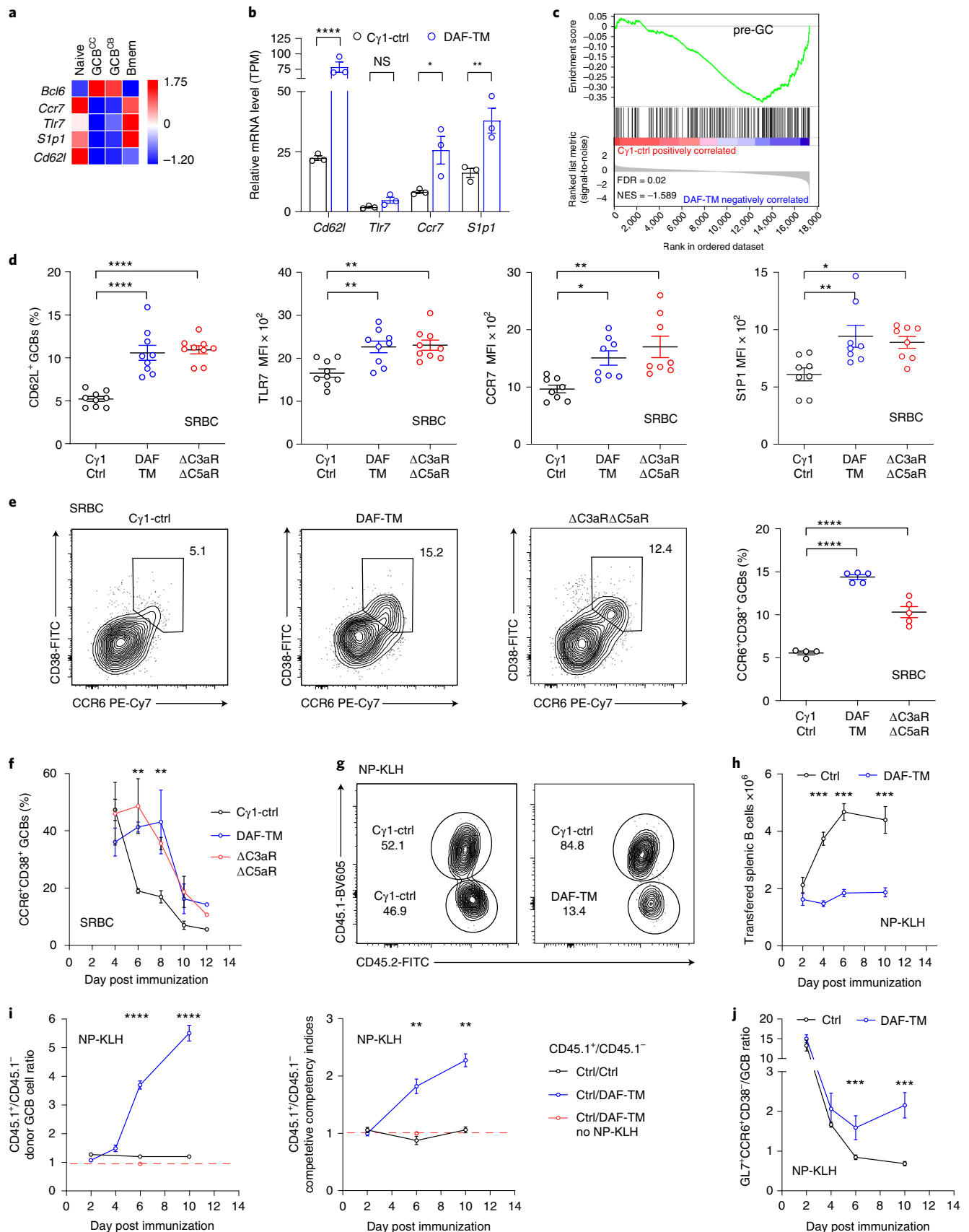
phosphorylation of the S6 ribosomal protein, pS6) 4 h after intravenous injection of either control IgG, anti-CD40, anti-IgM F(ab')$_2$ or anti-CD40+ anti-IgM F(ab')$_2$ antibodies (see Extended Data Fig. 8b–d for controls). Anti-CD40 + anti-IgM F(ab')$_2$ induced significant increases in pS6 (mTOR substrate) and MYC expression in WT GC B cells, with reduced responses in DAF-TM$^{C\gamma1}$ and ΔC3ar1/C5ar1$^{C\gamma1}$ GC B cells (Fig. 6b,c), despite comparable levels of CD40 and BCR (CD79, Igα/Igβ) expression among genotypes (Fig. 6d,e). To test whether these differences were confounded by binding of anti-IgM F(ab')$_2$ to circulating IgM, we performed analogous experiments by transfer of control or germline C3ar1$^{-/-}$C5ar1$^{-/-}$ B cells into IgM-deficient recipients (μMT[40]; Extended Data Fig. 8e,f). These assays confirmed that combined anti-CD40+/anti-IgM F(ab')$_2$ treatment induced pS6 upregulation in control B cells but failed to do so efficiently in C3ar1$^{-/-}$C5ar1$^{-/-}$ B cells (ELISA assays confirmed essentially absent serum IgM; Extended Data Fig. 8g).

Complementary in vitro experiments showed that the addition of recombinant C3a/C5a effectively induced mTOR signaling in WT GC (and naive) B cells exposed to CD40/IgM stimulation (Fig. 6f,g), but had no measurable effect on C3ar1/C5ar1-deficient B cells. C3a/C5a alone induced low levels of S6 protein phosphorylation in naive and GC B cells in the absence of anti-CD40/IgM (Extended Data Fig. 8h).

Discussion

The dynamic control of local complement activation, accomplished via alteration of surface complement regulator expression levels, represents an overlooked component of the GC gene program. Coordinated reprogramming of complement regulators on GC B cells allows enhanced C3a/C5a production and local B cell C3aR1–C5aR1 signaling, which directly contribute to B cell positive selection events required for GC formation, maintenance and function. Our data identify BCL6 as a crucial transcriptional repressor involved in this process, although contribution by other transcriptional controllers is possible. Our observations that (1) DAF is essentially absent on GC B cells, (2) transgenic DAF overexpression markedly alters GC responses in the absence of compensatory changes in the expression of other key regulators (for example, CR2, Crry or C5aR2) and (3) CR2 signaling contributes little in this antigen-rich setting[41] all suggest that BCL6-induced repression of DAF is vital for optimal GC function. While we did not genetically assess the impact of other complement regulators, it is conceivable that coordinated repression of DAF, CD46 (human) and CD21/35 is required for optimal initiation of GC B cell C3aR1–C5ar1 signaling. The simultaneous upregulation of CD59 (BCL6 independent) prevents MAC formation and probably inhibits B cell lysis despite upstream complement activation. CD59 upregulation on GC B cells probably contributes to GC B cell survival: others have shown that CD59-deficient mice develop weaker T-dependent antibody responses[42]. The positive effects of the FX1 BCL6 inhibitor on CD59 levels are possibly indirect (ChIP–seq showed no binding in regulatory regions).

Positive selection in GCs requires BCR activation and ligation of B cell CD40, along with signals initiated by cytokines and other ligands—for example, inducible T cell costimulator ligand[2–4]. While these concurrent signals induce mTORC1 activation and MYC

upregulation, their integration has remained incompletely understood. The finding that the absence of C3aR1–C5aR1 signaling in GC B cells results in severe defects in GC formation/maintenance and precludes effective activation of mTOR (and MYC expression), along with our previous studies linking C3aR1–C5aR1 to PI3-Kγ–AKT-dependent mTOR activation in other immune cells[9,10], strongly suggest that complement receptor-initiated signals are rate limiting and coalesce with other positive selection cues in B cells undergoing T cell–dependent positive selection. We surmise that the observed signaling defects during positive selection explain the major GC phenotypes in DAF-TM$^{C\gamma1}$ and ΔC3ar1/C5ar1$^{C\gamma1}$ mice, namely the competitive disadvantage and alterations in proliferation/death balance, as well as the defects in GC formation, maintenance and loss of affinity.

A notable finding is that expression of DAF-TM or absence of B cell C3aR1–C5aR1 signaling resulted in the accumulation of GL7$^+$ Fas$^+$ B cells expressing CD62L, TLR7, S1P1, CCR7 and CCR6, both at the transcript and protein level. Upregulation of these markers in GL7$^+$ cells has been reported not only in antigen-activated B cells before GC entry[5,29,43], but also in memory B cell precursors (typically with low antigen affinities)[44], while being specifically downregulated in GC B cells. This surface phenotype therefore precedes key cell fate transitions in mature B cells. Persistence of these markers in antigen-activated B cells from DAF-TM and C3aR1–C5aR1-null mice strongly suggests that, following activation by antigen and T cells, these B cells are incapable of completing such fate transitions. Accordingly, the progressive depletion of DAF-TM and C3ar1$^{-/-}$C5ar1$^{-/-}$ B cells in competitive chimeras suggests that these cells will be eventually lost to fitter wild-type B cells, thereby preventing their effective accumulation before GC entry (noting that we did not find any pre-GC clusters in tissue sections) or as early memory B cell precursors (noting that the overall numbers of definitive memory B cells are diminished).

The demonstration of an integral role for GC B cell-expressed DAF and C3aR1–C5aR1 signaling in the control of GC dynamics is distinct from other reported effects of complement in humoral immunity[11,26,45,46]. Ligation of B cell-expressed CD21 (CR2) by C3dg-coated antigen lowers naive B cell activation thresholds, in part by phosphorylation of CD19. This mechanism is most relevant for B cells responding to T-independent antigens, but not to T-dependent responses and, in contrast to our observed >90% reduction in antigen-specific serum antibody in the absence of C3aR1–C5aR1 signaling on B cells, CD21 deficiency reduces only modestly T cell–dependent humoral immune responses[41]. Other studies employing germline C3ar1/C5ar1-deficient animals showed that B cell-expressed C3aR1–C5aR1 signals drive early activation events (including upregulation of AID and BCL6), but potential links to GC dynamics and GC-dependent affinity maturation were not addressed[46]. A recent paper[47] reported DAF downregulation on human GC B cells, largely confirming our findings. The authors suggested that DAF downregulation would enhance phagocytosis of GC B cells and could possibly also facilitate interaction with T cells—mechanisms not directly tested in our study but that could directly or indirectly impact affinity maturation and positive selection in the GC[48,49], contributing to the phenotypes that we detected in our models.

Fig. 6 | DAF-TM and absence of C3aR–C5aR signaling in GC B cells reduce signals required for positive selection independently of CD40. a, GSEA enrichment plots for selected gene sets in DAF-TM$^{C\gamma1}$ versus Cγ1-Cre$^{+/-}$ mice. **b,c**, Representative histograms (left) and quantification (right) for MYC (**b**) and phosphorylated S6 (pS6) (**c**) in day 10 GCB cells isolated 4 h after in vivo stimulation with anti-CD40/IgM F(ab')$_2$ (see Extended Data Fig. 8b–d for controls). **d,e**, Quantified CD40 (MFI, **d**) and CD79 (Igα/Igβ, **e**) expression in GC B cells, day 10 post-SRBC immunization in DAF-TM, ΔC3aRΔC5aR and control Cγ1 Ctrl mice. **f,g**, Representative pS6 flow histograms (**f**) and quantified results (**g**) of naive (top) and GC B cells (bottom) from WT or germline C3ar1$^{-/-}$C5ar1$^{-/-}$ mice, stimulated in vitro for 20 min with subthreshold amounts of anti-CD40/IgM F(ab')$_2 \pm$ recombinant C3a and C5a proteins, as indicated (Extended Data Fig. 8h). **b–e,g**, Data are presented as MFI $\pm$ s.e.m.; $n = 5$–8 per group. **P < 0.01, ***P < 0.001, ****P < 0.0001 by ANOVA with Bonferroni post-test. Each dot represents one biological replicate.
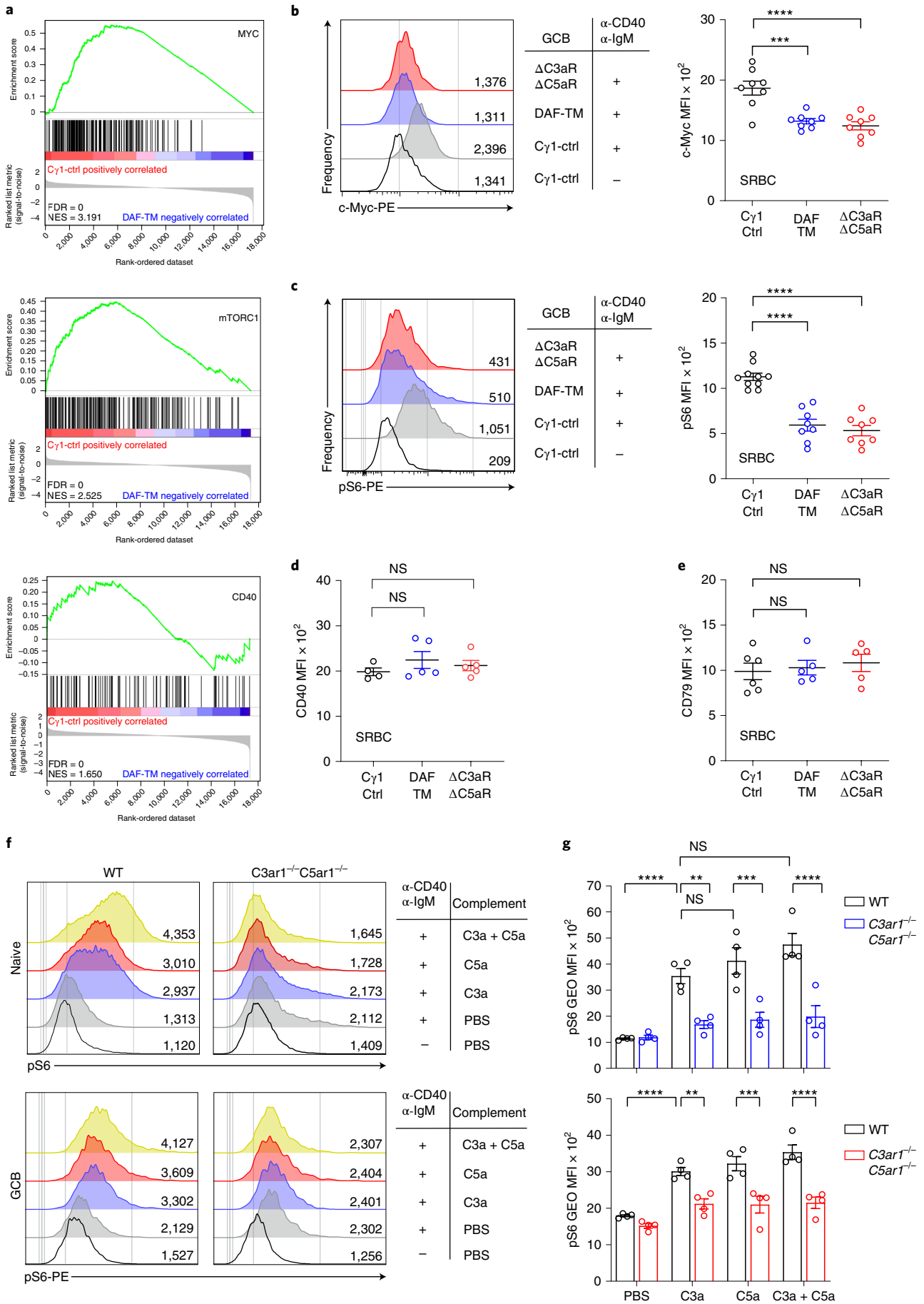
Key studies by Kemper and colleagues, among others, reported unanticipated roles for intracellular complement (that is, the complosome) in physiological T cell immune responses, particularly in humans[50,51]. Intracellular C3, C3a and C5a have been detected in human and murine B cells[46,51,52] and may contribute to early B cell activation[46], but we are not aware of any evidence that intracellular complement participates in GC responses. Our BM chimera studies indicate a dominant role for systemic C3 in the observed GC B cell effects, although we noted a subtle (albeit statistically significant) contribution of immune-cell-derived C3. The finding that GC responses are impaired in C1q-deficient, but not in factor-B-deficient or MBL-deficient, mice adds further mechanistic insight to the unexplained observation that C1q/BCR ligations contribute to successful GC responses[53]: in the context of physiologically downregulated DAF on GC B cells, C1q crosslinking of surface IgM and IgG may initiate complement activation and subsequent C3aR1–C5aR1 signaling required for optimal positive selection. Of note, C1q transcripts are specifically upregulated in positively selected MYC+ GC B cells[7], raising the possibility that this process could be dependent upon locally produced, rather than systemic, C1q.

Overall, our results support an enhanced view of complement signaling as an essential element of the humoral response, and indicate that the contribution of this signaling pathway to immunity is multifaceted, bridging pathways and regulatory modules involved in both innate and adaptive immune responses. Analyses of public databases show that, aside from GC B cells, BCL6 and DAF are also inversely expressed in DCs and neutrophils (Immunological Genome Project; Immgen.org), suggesting that coordinated repression of C3/C4 convertase regulators could enable modulation by local complement activation of other immune cell functions, with important implications beyond those regarding B cells. Our findings also identify unrecognized targets for therapeutic manipulation of humoral immunity in health and disease. Manipulation of complement signaling—particularly the complement regulator–C3aR1–C5aR1 axis here described—would facilitate the targeted modulation of adaptive immune responses in multiple settings: the design of vaccines, the management of transplants and, contextualizing our study with recent findings[54,55], in the modulation of immune responses to cancer.

Online content

Any methods, additional references, Nature Research reporting summaries, source data, extended data, supplementary information, acknowledgements, peer review information; details of author contributions and competing interests; and statements of data and code availability are available at https://doi.org/10.1038/s41590-021-00926-0.

References

1. Victora, G. D. & Nussenzweig, M. C. Germinal centers. *Annu. Rev. Immunol.* **30**, 429–457 (2012).
2. Shlomchik, M. J., Luo, W. & Weisel, F. Linking signaling and selection in the germinal center. *Immunol. Rev.* **288**, 49–63 (2019).
3. Ersching, J. et al. Germinal center selection and affinity maturation require dynamic regulation of mTORC1 kinase. *Immunity* **46**, 1045–1058 (2017).
4. Luo, W., Weisel, F. & Shlomchik, M. J. B cell receptor and CD40 signaling are rewired for synergistic induction of the c-Myc transcription factor in germinal center B cells. *Immunity* **48**, 313–326 (2018).
5. Schwickert, T. A. et al. A dynamic T cell–limited checkpoint regulates affinity-dependent B cell entry into the germinal center. *J. Exp. Med.* **208**, 1243–1252 (2011).
6. Srinivasan, L. et al. PI3 kinase signals BCR-dependent mature B cell survival. *Cell* **139**, 573–586 (2009).
7. Dominguez-Sola, D. et al. The proto-oncogene *MYC* is required for selection in the germinal center and cyclic reentry. *Nat. Immunol.* **13**, 1083–1091 (2012).
8. Heeger, P. S. et al. Decay-accelerating factor modulates induction of T cell immunity. *J. Exp. Med.* **201**, 1523–1530 (2005).
9. Lalli, P. N. et al. Locally produced C5a binds to T cell–expressed C5aR to enhance effector T-cell expansion by limiting antigen-induced apoptosis. *Blood* **112**, 1759–1766 (2008).
10. Strainic, M. G. et al. Locally produced complement fragments C5a and C3a provide both costimulatory and survival signals to naive CD4+ T cells. *Immunity* **28**, 425–435 (2008).
11. Verghese, D. A. et al. C5aR1 regulates T follicular helper differentiation and chronic graft-versus-host disease bronchiolitis obliterans. *JCI Insight*, https://doi.org/10.1172/jci.insight.124646 (2018).
12. Medof, M. E., Kinoshita, T. & Nussenzweig, V. Inhibition of complement activation on the surface of cells after incorporation of decay-accelerating factor (DAF) into their membranes. *J. Exp. Med.* **160**, 1558–1578 (1984).
13. Carroll, M. C. et al. Organization of the genes encoding complement receptors type 1 and 2, decay-accelerating factor, and C4-binding protein in the RCA locus on human chromosome 1. *J. Exp. Med.* **167**, 1271–1280 (1988).
14. Jacobson, A. C. & Weis, J. H. Comparative functional evolution of human and mouse CR1 and CR2. *J. Immunol.* **181**, 2953–2959 (2008).
15. Kennedy, D. E. et al. Novel specialized cell state and spatial compartments within the germinal center. *Nat. Immunol.* **21**, 660–670 (2020).
16. Basso, K. & Dalla-Favera, R. Roles of BCL6 in normal and transformed germinal center B cells. *Immunol. Rev.* **247**, 172–183 (2012).
17. Kitano, M. et al. Bcl6 protein expression shapes pre-germinal center B cell dynamics and follicular helper T cell heterogeneity. *Immunity* **34**, 961–972 (2011).
18. Dominguez-Sola, D. et al. The FOXO1 transcription factor instructs the germinal center dark zone program. *Immunity* **43**, 1064–1074 (2015).
19. Basso, K. et al. Integrated biochemical and computational approach identifies BCL6 direct target genes controlling multiple pathways in normal germinal center B cells. *Blood* **115**, 975–984 (2010).
20. Cardenas, M. G. et al. Rationally designed BCL6 inhibitors target activated B cell diffuse large B cell lymphoma. *J. Clin. Invest.* **126**, 3351–3362 (2016).
21. Rickert, R. C., Roes, J. & Rajewsky, K. B lymphocyte-specific, Cre-mediated mutagenesis in mice. *Nucleic Acids Res.* **25**, 1317–1318 (1997).
22. Casola, S. et al. Tracking germinal center B cells expressing germ-line immunoglobulin γ1 transcripts by conditional gene targeting. *Proc. Natl Acad. Sci. USA* **103**, 7396–7401 (2006).
23. Lalli, P. N., Strainic, M. G., Lin, F., Medof, M. E. & Heeger, P. S. Decay accelerating factor can control T cell differentiation into IFN-γ-producing effector cells via regulating local C5a-induced IL-12 production. *J. Immunol.* **179**, 5793–5802 (2007).
24. Verghese, D. A. et al. T cell expression of C5a receptor 2 augments murine regulatory T cell (T_REG) generation and T_REG-dependent cardiac allograft survival. *J. Immunol.* **200**, 2186–2198 (2018).
25. Mayer, C. T. et al. The microanatomic segregation of selection by apoptosis in the germinal center. *Science* **358**, eaao2602 (2017).
26. Hebell, T., Ahearn, J. M. & Fearon, D. T. Suppression of the immune response by a soluble complement receptor of B lymphocytes. *Science* **254**, 102–105 (1991).
27. Wentink, M. W. et al. CD21 and CD19 deficiency: two defects in the same complex leading to different disease modalities. *Clin. Immunol.* **161**, 120–127 (2015).
28. Jolly, C. J., Klix, N. & Neuberger, M. S. Rapid methods for the analysis of immunoglobulin gene hypermutation: application to transgenic and gene targeted mice. *Nucleic Acids Res.* **25**, 1913–1919 (1997).
29. Inoue, T. et al. The transcription factor Foxo1 controls germinal center B cell proliferation in response to T cell help. *J. Exp. Med.* **214**, 1181–1198 (2017).
30. Pereira, J. P., Kelly, L. M., Xu, Y. & Cyster, J. G. EBI2 mediates B cell segregation between the outer and centre follicle. *Nature* **460**, 1122–1126 (2009).
31. Klein, U. et al. Transcriptional analysis of the B cell germinal center reaction. *Proc. Natl Acad. Sci. USA* **100**, 2639–2644 (2003).
32. Gatto, D., Wood, K. & Brink, R. EBI2 operates independently of but in cooperation with CXCR5 and CCR7 to direct B cell migration and organization in follicles and the germinal center. *J. Immunol.* **187**, 4621–4628 (2011).
33. Cyster, J. G. et al. Follicular stromal cells and lymphocyte homing to follicles. *Immunol. Rev.* **176**, 181–193 (2000).
34. Green, J. A. et al. The sphingosine 1-phosphate receptor S1P₂ maintains the homeostasis of germinal center B cells and promotes niche confinement. *Nat. Immunol.* **12**, 672–680 (2011).
35. Gatto, D., Paus, D., Basten, A., Mackay, C. R. & Brink, R. Guidance of B cells by the orphan G protein-coupled receptor EBI2 shapes humoral immune responses. *Immunity* **31**, 259–269 (2009).
36. Zhao, R. et al. A GPR174–CCL21 module imparts sexual dimorphism to humoral immunity. *Nature* **577**, 416–420 (2020).
37. Lu, P., Shih, C. & Qi, H. Ephrin B1–mediated repulsion and signaling control germinal center T cell territoriality and function. *Science* **356**, eaai9264 (2017).

38. Pae, J. et al. Cyclin D3 drives inertial cell cycling in dark zone germinal center B cells. *J. Exp. Med.* **218**, 20201699 (2021).

39. Subramanian, A. et al. Gene set enrichment analysis: a knowledge-based approach for interpreting genome-wide expression profiles. *Proc. Natl Acad. Sci. USA* **102**, 15545–15550 (2005).

40. Kitamura, D., Roes, J., Kuhn, R. & Rajewsky, K. A B cell-deficient mouse by targeted disruption of the membrane exon of the immunoglobulin mu chain gene. *Nature* **350**, 423–426 (1991).

41. Ahearn, J. M. et al. Disruption of the *Cr2* locus results in a reduction in B-1a cells and in an impaired B cell response to T-dependent antigen. *Immunity* **4**, 251–262 (1996).

42. Sivasankar, B. et al. CD59a deficient mice display reduced B cell activity and antibody production in response to T-dependent antigens. *Mol. Immunol.* **44**, 2978–2987 (2007).

43. Wiede, F. et al. CCR6 is transiently upregulated on B cells after activation and modulates the germinal center reaction in the mouse. *Immunol. Cell Biol.* **91**, 335–339 (2013).

44. Suan, D. et al. CCR6 defines memory B cell precursors in mouse and human germinal centers, revealing light-zone location and predominant low antigen affinity. *Immunity* **47**, 1142–1153 (2017).

45. Carroll, M. C. & Isenman, D. E. Regulation of humoral immunity by complement. *Immunity* **37**, 199–207 (2012).

46. Paiano, J. et al. Follicular B2 cell activation and class switch recombination depend on autocrine C3ar1/C5ar1 signaling in B2 cells. *J. Immunol.* **203**, 379–388 (2019).

47. Dernstedt, A. et al. Regulation of decay accelerating factor primes human germinal center B cells for phagocytosis. *Front. Immunol.* **11**, 599647 (2020).

48. Biram, A., Davidzohn, N. & Shulman, Z. T cell interactions with B cells during germinal center formation, a three-step model. *Immunol. Rev.* **288**, 37–48 (2019).

49. Wu, Y. L. & Rada, C. Molecular fine-tuning of affinity maturation in germinal centers. *J. Clin. Invest.* **126**, 32–34 (2016).

50. Arbore, G. et al. T helper 1 immunity requires complement-driven NLRP3 inflammasome activity in CD4+ T cells. *Science* **352**, aad1210 (2016).

51. Liszewski, M. K. et al. Intracellular complement activation sustains T cell homeostasis and mediates effector differentiation. *Immunity* **39**, 1143–1157 (2013).

52. West, E. E., Afzali, B. & Kemper, C. Unexpected roles for intracellular complement in the regulation of Th1 responses. *Adv. Immunol.* **138**, 35–70 (2018).

53. Rossbacher, J. & Shlomchik, M. J. The B cell receptor itself can activate complement to provide the complement receptor 1/2 ligand required to enhance B cell immune responses in vivo. *J. Exp. Med.* **198**, 591–602 (2003).

54. Bird, L. Switch to antitumour B cells. *Nat. Rev. Immunol.* **20**, 274–275 (2020).

55. Lu, Y. et al. Complement signals determine opposite effects of B cells in chemotherapy-induced immunity. *Cell* **180**, 1081–1097 (2020).

56. Heng, T. S. et al. The Immunological Genome Project: networks of gene expression in immune cells. *Nat. Immunol.* **9**, 1091–1094 (2008).

57. Zhang, J. et al. Disruption of KMT2D perturbs germinal center B cell development and promotes lymphomagenesis. *Nat. Med.* **21**, 1190–1198 (2015).

Methods

Mice. C57BL/6/J (B6, catalog no. 000664), B6;129S4-*C3tm1Crr*/J (*C3tm1Crr*, C3−/−, catalog no. 029661), B6.129P2(C)-*Cd19tm1(cre)Cgn*/J (catalog no. 6785, *CD19*-Cre+/−), C.129P2(Cg)-*Ighg1tm1(cre)Cgn*/J (catalog no. 010611), *Cγ1*-Cre+/−, B6.SJL-*Ptprca Pepcb*/BoyJ (catalog no. 002014, CD45.1) and B6.129S2-*Ighmtm1Cgn*/J (catalog no. 002288, μMT) mice, all *H-2b*, were purchased from Jackson Laboratory (Jax) and bred at the Icahn School of Medicine at Mount Sinai. Experiments using *CD19*-Cre+/− and *Cγ1*-Cre+/− knock-in models were performed using Cre+/− heterozygotes. Germline B6 *C3ar1*−/−*C5ar1*−/− mice were generated as described[13,15].

The following animals (mice) were kind gifts: B6.129S4-*Mbl1tm1Kata Mbl2tm1Kata*/J (*mbl1*−/−*mbl2*−/−) from G. Stahl (Harvard Medical School); complement factor B−/−, produced by M. Pekna (Gothenburg, Sweden), from M. Zhang (SUNY Downstate); *Cr1*−/− (CD21-deficient) produced by M. Carroll (Harvard Medical School)[58] (SUNY Downstate); B6(Cg)-*C1qatm1d(EUCOMM)Wtsi*/TennJ (Jax, catalog no. 031675, *C1q*−/−) from B. Diamond (Feinstein Institute, Northwell Health); *BCL6YFP*mice[17] generated by T. Okada (Kyoto University, Kyoto, Japan), from S. Reiner, (Columbia University); and B18hi BCR transgenic mice from M. Nussenzweig (Rockefeller University).

B6 *C5ar1*fl/fl mice were described previously[59]. B6 *C3ar1*fl/fl mice were generated from embryonic stem cells purchased from the EUCOMM consortium. The Mouse Genetics core facility at Icahn School of Medicine at Mount Sinai injected the *C3ar1*fl/fl embryonic stem cells into pseudopregnant B6 mice using standard techniques. After validation of founder genotype, the animals were crossed to B6.129S4-*Gt(ROSA)26Sortm2(FLP*)Sor*/J mice (Jax, catalog no. 012930) to remove the neocassette. *C5ar1*fl/fl and *C3ar1*fl/fl animals were crossed with *Cγ1*-Cre transgenics to produce *C3ar1*fl/fl×*Cγ1*-Cre+/− and *C5ar1*fl/fl×μ*Cγ1*-Cre+/− mice, and then intercrossed to produce *C3ar*fl/fl/*C5ar1*fl/fl×*Cγ1*-Cre+/− (Δ*C3ar1/C5ar1Cγ1*) mice.

All animals were housed in the Center for Comparative Medicine and Surgery at the Icahn School of Medicine at Mount Sinai, under the Institutional Animal Care and Use Committee (IACUC) in accordance with guidelines of the Association for Assessment and Accreditation of Laboratory Animal Care International. Mice were housed under pathogen-free conditions at 22 °C and 30–70% humidity in a 12/12-h light/dark cycle and provided ad libitum access to food and water. Experiments were performed in compliance with ethical guidelines under IACUC approval no. 2018-0084 (approved February 2018). Experiments were performed with groups of age- (6–12 weeks) and sex-matched mice, using littermates or animals maintained in the same room and cohoused within the same cages for >2 weeks.

Generation of conditional DAF-TM transgenic mice. The DAF-TM transgenic gene (Extended Data Fig. 3) was constructed using the coding sequence of the mouse *Daf1* gene (*Cd55*) containing the complement regulatory domain[60], replacing the signal sequence for GPI-anchor addition with that of the transmembrane helix domain of human tissue factor (nonsignaling; Extended Data Fig. 3). Transgene expression driven by the CAG promoter in the *Rosa26* locus is regulated by a loxP flanked transcriptional stop element.

Paired Cas9D10A nickase (Cas9n) was used to target the transgene into the *Rosa26* locus (for details on targeting sequences, see Extended Data Fig. 3a: ACTGGAGTTGCAGATCACGA GGG, GGCAGGCTTAAAGGCTAACC TGG). The guide RNA-A and gRNA-B sequences were inserted into two separate plasmid constructs on the pX460 (Addgene) backbone, both also containing a copy of the Cas9n coding sequence. A pUC57_DAF-TM homology repair plasmid was prepared comprising the DAF-TM transgenic construct flanked by *Rosa26* homology arms. Purified plasmid DNA constructs from transformed *Escherichia coli* (Invitrogen/ThermoFisher), using the EndoFree Plasmid Maxi kit (Qiagen), were verified by sequencing, transferred into fertilized DBA2/B6 F1 hybrid eggs[61] by pronuclear microinjection (0.75 ng μl−1 per gRNA, 10 ng μl−1 of repair template) and injected into pseudopregnant animals at the Mouse Genomics Core Facility (Mount Sinai).

Transgene presence was verified in founders by PCR using primers (5′–AGTCTGATGTAGGACAATGGAG–3′, 5′–AGGATGATGACCACAAATACC–3′) specific for the chimeric junction within the DAF-TM gene segment unique to the mouse genome. Correct site-specific integration was determined by junction PCR reactions using primer pairs (5′–AGCGGAAACGCCACTGAC–3′, 5′–GGGCGT ACTTGGCATATGAT–3′ and 5′–AGTCTGATGTAGGACAATGGAG–3′, 5′–GC TCCTCTGTCCACAGTTACA –3′), spanning genomic and transgenic sites at both ends of the transgene.

Founder mice were backcrossed to C57BL/6 J for more than eight generations and then intercrossed with either *Cγ1*-Cre or *CD19*-Cre animals. All experiments within the study were performed with DAF-TM+/+ mice heterozygous for either *CD19*-Cre or *Cγ1*-Cre. DAF-TM zygosity was determined using PCR primers specific for the chimeric junction part of the transgene (see primers above), and primers for the intact *Rosa26* target integration site (5′–CGACTTGAGTTG CCTCAAGAG–3′ and 5′–CCAGATGACTACCTATCCTCC–3′).

Human tissue samples. Human tonsils were obtained as either deidentified, discarded surgical specimens or deidentified, archived tissue samples, with approval of the Institutional Review Board at Mount Sinai Hospital (nos. BRC 272 and IRB 11-0178), from routine tonsillectomies performed at Mount Sinai Hospital

from the Biorepository and Pathology core. As such, the study is not considered human subject research under current NIH guidelines.

Cell lines. The human myeloma cell line KMS was purchased from the Japanese Collection of Research Bioresources Cell Bank (https://cellbank.nibiohn.go.jp/english/). The human diffuse large B cell lymphoma (DLBCL) cell lines SU-DHL-5, SU-DHL-6, SU-DHL-10, OCI-LY7 and TOLEDO, and the Burkitt lymphoma cell line P3HR1, were gifts of L. Pasqualucci (Columbia University Medical Center) and originally purchased from the DSMZ (www.dsmz.de) repository (SU-DHL lines and OCI-LY7) or American Type Culture Collection (ATCC; atcc.org) (P3HR1 and TOLEDO). Cell line identities were confirmed by multiplex cell authentication (Genetica Cell Line Testing). KMS-27 cells were cultured in RPMI 1640 medium (Life Technologies) plus 20% heat-inactivated fetal bovine serum (FBS, Life Technologies) and 1% penicillin/streptomycin (Life Technologies). Lymphoma cell lines were cultured in Iscove modified Dulbecco's medium (Life Technologies), 10% FBS (Life Technologies) and 1% penicillin/streptomycin.

Mouse immunization. Groups of animals were immunized with either SRBC (Innovative Research) or NP-KLH (BioSearch Technologies). For SRBC immunization, either a single intraperitoneal injection of 1 × 10^9 SRBC or sequential SRBC injections (day 0, 1–2×10^8; day 5, 1 × 10^9) were used as indicated. For NP-KLH, 100 μg of NP-KLH (1:1 vol/vol) in alum (Immject Alum, ThermoFisher) was precipitated and injected intraperitoneally.

Bone marrow chimeras. Reciprocal WT CD45.1 and (CD45.2) C3−/− bone marrow chimeras were produced as published[62]. Eight weeks after engraftment, >95% peripheral blood donor chimerism was confirmed before immunization.

ELISA assay. Anti-SRBC titers were determined using an ELISA kit (Innovative Research) to assess high-affinity and total anti-NP antibodies using bovine serum albumin (BSA) with different degrees of NP conjugation[63].

DAF cleavage and complement deposition assay. Splenocytes (5×10^6) from NP-KLH mice were incubated in HL-1-serum-free medium (Lonza) for 1 h at 37 °C and 5% CO2 in the presence or absence of 5 μg ml−1 Phospholipase C (Sigma-Aldrich), washed with PBS and 1% fetal calf serum (FCS), and surface DAF expression was quantified by flow cytometry. The complement regulatory capacity of DAF-TM was assessed in vitro by incubation of 5×10^6 splenocytes from immunized animals in 20–40% WT or C3−/− mouse serum in Annexin V buffer with 1 mM MgCl2 for 20 min at 37 °C, 5% CO2 and quantification of C3b deposition by flow cytometry.

In vitro and in vivo GC B cell stimulation. *In vivo stimulation.* Ten days after immunization of groups of control *Cγ1*-Cre+/−, DAF-TMCγ1 and Δ*C3ar1/C5ar1Cγ1* mice with SRBC, animals were injected intravenously with anti-CD40 (150 μg) and/or anti-IgM F(ab′)2 (100 μg), or goat IgG2a (all from BioXcell) in 200 μl of PBS. Spleens were harvested at 4 h for surface staining followed by fixation, permeabilization and intracellular staining. In other studies, 20×10^6 B6 WT or C3aR1−/−C5aR1−/− B cells were transferred into μMT recipients, and 24 h later, recipients were immunized with SRBC. On day 10, animals were injected with anti-CD40 (150 μg) and/or anti-IgM F(ab′)2 (100 μg) or control goat IgG2a and the cells analyzed by flow cytometry. Serum IgM was quantified with an IgM Mouse Uncoated ELISA kit (Invitrogen).

For in vitro studies, 10 days after sequential SRBC immunization, isolated spleen cells were enriched (B cell Magnisort kit, ThermoFisher), rested for 20 min at 37 C, 5% CO2 in HL-1 medium and subsequently stimulated with 10 μg ml−1 anti-CD40, 10 μg ml−1 anti-IgM and 0.5 μg ml−1 murine C3a and/or C5a for 20 min at 37 C, 5% CO2. After washing, cells were stained and analyzed by flow cytometry.

In vivo competition studies. Equal numbers (10^7 each) of purified CD45.2 B1-8hi DAF-TM *Cγ1*-Cre+/− B cells (or, in control experiments, CD45.2 B1-8hi *Cγ1*-Cre+/−) and control CD45.1/2 B1-8hi *Cγ1*-Cre+/− B cells were injected into CD45.1 B6 recipients. Twenty-four hours later (day 0), recipient mice were immunized with 100 mg of NP-KLH, except for a set of four animals used as nonimmunized control. Groups of animals were sacrificed at days 0, 6 and 9 post immunization, and isolated splenic mononuclear cells were analyzed by flow cytometry. Competitive competency indices were calculated as the percentage of each population in GCs, normalized to that in non-GC B cell fractions. This normalization minimizes the impact of varied engraftment among congenic cells in individual mice[37].

Immunofluorescence analysis. Fixed human tonsil tissue fragments and murine draining lymph nodes and spleens (1.6% PFA and 20% sucrose, 4 h to overnight at 4 °C) were incubated in PBS and 15% sucrose overnight, with rotation at 4 °C, embedded in optimum cutting temperature compound (Tissue Tek, Sakura Finetek), cut into 8-μm sections, fixed in cold acetone for 5 min at room temperature then blocked in 3% BSA (Sigma-Aldrich). Sections were incubated with anti-CD35 (fluorescein isothiocyanate (FITC)), anti-GL7 (PE) and anti-IgD (APC) antibodies for 2 h at room temperature in blocking solution, washed with

PBS and counterstained with DAPI (Vectashield, Vector Laboratories). Images were captured using a fluorescence microscope and NIS-Elements v.4.20 imaging software (Nikon).

Plasmids. A pMT2T backbone was used to express full-length and truncated human BCL6 variants in transient luciferase reporter assays. Truncated variants encode BCL6 mutants[64] lacking either the amino-terminal transcriptional repressor domain (BCL6-ZF) or the carboxy-terminal DNA binding zinc-finger domain (BCL6-ΔZF), all a kind gift of K. Basso, Q. Shen and R. Dalla-Favera (Columbia University). To generate a CD55 reporter construct, PCR-amplified genomic regions spanning the human CD55 promoter (chr1:207,320,781-207,321,774; hg38 assembly) and an intronic enhancer (chr1:207,335,687-207,337,273, hg38) were subcloned into BamHI/SalI sites of pNL3.1 (Nluc minP, Promega). The promoter region, including the 5′ UTR up to the ATG upstream of the NanoLuc complementary DNA (Nluc), was subcloned into pNL3.1 (HindIII/NcoI), replacing the ATG of Nluc with that of CD55. Promoter and enhancer regions were defined based on the span of H3K27ac and H3K4me1/3 marks in ChIP–seq datasets (Fig. 2b and Extended Data Fig. 2).

TRE3G-BCL6-puromycin and TRE3G-BCL6-ZF-puromycin lentiviral vectors were constructed by subcloning a cDNA encoding full-length human BCL6, or a truncated cDNA encoding the zinc-finger DNA binding domain (ZF) downstream of a TRE3G promoter element in a modified version of pZIP-TRE3G (TransOmic). The modified vector has a UbC-rtTA-IRES-Puro cassette; all BCL6 cDNAs were subcloned 3′ of TRE3G via Gibson assembly (NEBuilder HiFi DNA Assembly Cloning kit, New England Biolabs). BCL6 expression is responsive to (that is, induced by) the addition of doxycycline (Dox). All vector DNA and sequences are available upon request.

Electroporation and reporter assay. TOLEDO cells (4×10^5) were electroporated and resuspended in buffer R (Life Technologies) using the Neon Electroporation Transfection System (Life Technologies) (10-μl tip, 1,350 V, one pulse of 40 ms). In all transfections, 390 ng of the recombinant CD55-prom-enh-Nluc was combined with either the indicated amounts of pMT2T-BCL6 or 100 ng of pMT2T-BCL6-ZF/pMT2T-BCL6-ΔZF, a Firefly luciferase encoding vector (pGL4.13, Promega), to control for electroporation efficiency, and pUC19 vector (NEB), for a total of 500 ng. Electroporated cells ($4 \times 10^5\,ml^{-1}$) were cultured in IMDM/10% FBS without antibiotics, and luciferase levels were measured 48 h post transfection using the Nano-Glo Dual-Luciferase Reporter Assay System (Promega). Reporter activity was reported as the ratio between Nanoluc and Firefly (transfection control) luciferase readings in multiple technical replicates across $n > 3$ experimental replicates. Statistical significance was calculated based on the average of technical replicates in each experiment, using Student's t-test (unpaired, two-tailed).

Lentiviral packaging and cell transduction. To generate TRE3G-puro lentiviral particles, HEK293T cells (ATCC) were reverse transfected with TRE3G-puro lentiviral vector encoding BCL6 or BCL6-ZF and packaging vectors encoding REV, TAT, VSVG and GAG-Pol (10:1:1:2:1, for a total of 15 μg) in a 1-ml solution of 150 mM NaCl plus 1 μg μl^{-1} solution of polyethylenimine (PEI, Fisher Scientific), for a 1:4 DNA/PEI ratio. The DNA/PEI mixture was used for reverse transfection of 14×10^6 HEK293T cells in 100-mm^2 plates, incubated at 37 °C. Virus-containing supernatants were harvested in two consecutive collections on days 3 and 4, concentrated using Lenti-X concentrator (Clontech/Takara Bio) and resuspended in 1× PBS (100× suspension).

For human BCL6 overexpression, KMS-27 cells were transduced with lentiviral particles of TRE3G-BCL6-puro at high multiplicity of infection (MOI), and selected in 1 μg ml^{-1} puromycin to obtain cell pools with stable integration of the inducible transgene. Cells were cultured (1×10^6 cells in 2 ml of growth medium per well) in six-well plates, with 2 μg ml^{-1} Dox added to induce BCL6 expression. Cells were harvested at 72 h post induction, stained for CD55, CD46 and CD59, fixed and permeabilized in FoxP3 staining buffer (ThermoFisher Scientific/eBioscience), stained with phycoerythrin-conjugated anti-BCL6 antibody then analyzed by flow cytometry (FACSCalibur or Fortessa analyzer, BD).

For experiments using the dominant negative BCL6, SU-DHL-5 cells were transduced with TRE3G-BCL6-ZF-puro lentiviral particles at high MOI and selected with 1 μg ml^{-1} puromycin for stable integration. To induce BCL6-ZF expression, 5×10^5 cells were cultured in 2 ml of growth medium ±2 μg ml^{-1} Dox and harvested 72 h post induction. Next, 3×10^6 cells were used to confirm overexpression of the BCL6-ZF truncation by immunoblot, using a mouse monoclonal (H12) antibody directed against the C terminus (ZF) domain of BCL6.

In selected experiments, 25–50 μM BCL6 inhibitor FX1 (Selleck Chemicals), dissolved in dimethyl sulfoxide, was added to exponentially growing cultures of different DLBCL and BL cell lines in fresh growth medium. Cells were harvested at 24–48 h for flow cytometry analyses with specific anti-DAF and anti-CD46 antibodies (Supplementary Table 3).

Immunoblot. Cells were lysed in 1% SDS lysis buffer (50 mM Tris pH 8.0, 1 mM EDTA, 100 mM NaCl, 5 mM DTT and 1% SDS) containing protease and phosphatase inhibitors (ThermoFisher). Lysates (10–20 μg) were resolved in Bolt 4–12% Bis-Tris Plus gels (ThermoFisher) and MOPS buffer, transferred to nitrocellulose membranes (GE Healthcare) then incubated overnight at 4 °C with primary antibodies to BCL6 and β-actin (Supplementary Table 3). After washing and the addition of horseradish peroxidase-conjugated secondary antibodies (Kindle Biosciences), assays were developed using KwikQuant Ultra Digital ECL (Kindle Biosciences). Luminescent signal was detected using a FujiFilmX-A2digital camera, and raw images converted to black and white with Adobe Photoshop CS6 v.13.0.

Flow cytometry and cell sorting. Mouse spleen cell suspensions in RPMI medium were filtered (70 μm) and RBCs lysed (ACK buffer, Lonza), then refiltered (40 μm) to produce single mononuclear cell suspensions in PBS plus 1% FCS. For primary murine and human cells, as well as cell lines, surface and intracellular staining was performed using antibodies listed in Supplementary Table 3. Analyses were performed on either a FACS Lyric or Canto II cytometer (BD Biosciences) and the results analyzed with FlowJo software v.10.6.2 (FlowJo, LLC).

GCB cells from the spleens of SRBC-immunized mice were sorted after enrichment by negative selection using the MagniSort Mouse B Cells Enrichment Kit (ThermoFisher Scientific), with the addition of anti-IgD-biotin antibody to deplete IgD$^+$ naive cells. GC B cell pools were sorted using GL7$^+$FAS$^+$ (*Cγ1*-cre$^{+/-}$ control mice) and GL7$^+$FAS$^+$ DAF$^+$ (DAF-TM^{Cγ1} mice) in a BD FACS Aria III. DAF expression was used in the GL7$^+$/FAS$^+$ fraction to confirm transgene expression and successful recombination. In other analyses, cells in synthesis phase were labeled in vivo for 2 h following intravenous injection with 1 mg of EdU[65]. Cells in synthesis phase were gated as BrdU$^+$ 7AAD^{int}.

Assessment by BCR–sequencing of somatic hypermutation events in Vh186.2 mouse variable heavy-chain regions and JH4 intron. Ig-λ$^+$ GC B cells (1×10^4) were flow sorted) from DAF-TM^{Cγ1}, ΔC3ar1/C5ar1^{Cγ1} and control mice 12 days post immunization with 100 μg of NP-KLH, and genomic DNA was isolated using the QIAamp DNA Micro Kit (Qiagen). The variable heavy-chain region 186.2 with heavy-chain region 2 segments (Vh186.2-JH2, selected in GC response to NP immunization[66]) was amplified by PCR using specific primer sets and 10 ng of genomic DNA and KAPA HiFi DNA Polymerase (Kapa Biosystems-Roche). The PCR protocol was performed as previously described[5] and uses a seminested PCR (first PCR: outer forward primer, 5′-TCTTTACAGTTACTGAGCACACAGGAC-3′ and reverse primer, 5′-GGGTCTAGAGGTGTCCCTAGTCCTTCATGACC-3′; second PCR: inner forward primer 5′-CAGTAGCAGGCTTGAGGTCTGGAC-3′ and the same reverse primer). All final PCR products were subcloned into pCR-Blunt vector (Zero Blunt PCR Cloning Kit, Life Technologies), and single colonies Sanger sequenced (~40 per mouse) using a M13F-21 primer. Variable heavy-chain gene sequences were analyzed using HighV-Quest (The International Immunogenetics Information System)[67,68], identifying unique sequences (clones) matching the V186.2 gene (IGHV1-72*01). Differences in the frequency of clones with high-affinity mutations between groups were determined using Fisher's exact test. A chi-square test was used to compare total mutations within VH segments and mutation frequency per 100 base pairs (bp) in different groups. Statistical differences in the total number of mutations per segment were calculated using a Mann–Whitney test.

For the sequencing and analysis of hypermutation events at JH4 intronic regions, a 591-bp region from genomic DNA was amplified for 35 cycles using a high-fidelity polymerase (KAPA HiFi, KAPA Biosystems-Roche) and the following gene-specific primers[69]: *JH4int-F*: TCCTAGGAACCAACTTAAGAGT; *JH4int-R*: TGGAGTTTTCTGAGCATTGCAG. The products were cloned in the pCR-Blunt II vector (Zero Blunt PCR cloning kit, ThermoFisher) and sequenced using M13 primers by Sanger sequencing (~20–25 clones per mouse, three mice per genotype). All identical sequences were removed using ElimDupes (https://www.hiv.lanl.gov/content/sequence/elimdupesv2/elimdupes.html) and unique sequences were aligned to a consensus reference sequence using SHMTool[69]. The sequence in *Cγ1*-Cre mice differs from the C57BL/6 germline sequence at five nucleotide positions. Statistical significance in mutation frequencies was determined using the Mann–Whitney test (Graphpad Prism, v.8.4.2). Supplementary Table 1 provides a detailed summary of BCR–sequencing (BCR–seq) results.

RNA isolation and quality control. Total RNA was isolated from sorted, viable GC B cells (B220$^+$GL7$^+$Fas$^+$) from *Cγ1*-cre$^{+/-}$ control and DAF-TM^{Cγ1} mice using the Direct-zol RNA MicroPrep kit (Zymo Research). Purified RNA was eluted in DNase/RNase-free water, quantified by NanoDrop spectrophotometry and quality assessed (RNA integrity number) on an Agilent 2100 Bioanalyzer using a RNA 600 Pico kit.

RNA-seq. Total RNA (10 ng) was processed with RNA integrity number scores >5 to generate libraries for RNA-seq using the SMART-seq v.4 Ultra Low Input RNA kit (Takara). Libraries were multiplexed and sequenced on an Ilumina NextSeq 550 instrument, to a minimum of 30 million single-end 100-bp reads. HISAT2 v.2.1.0 (ref. [70]) was used to align Fastq reads to the *Mus musculus* genome (mm10) with options –dta –trim5 5 –add-chrname –ignore-quals -q -k 1; and featureCounts[71] with options -T -4 -exon -g gene_name, to generate raw counts from aligned BAM files. Raw read counts were used as input for differential expression analysis using

DESeq2 v.1.10.1 (ref. [72]). The table output of DESeq2 (82 genes, adjusted $P < 0.05$; Supplementary Table 2) was utilized for pathway enrichment analyses using either (1) the Broad Institute Molecular Signatures Database (Interrogate gene sets tool, hypergeometric distribution of P values) or (2) the Gene Set Enrichment Analysis tool (GSEA v.4.0.3)[39] with selected signatures (Figs. 5 and 6 and Extended Data Fig. 7), with the following settings: 'Permutations' -gene set; 'Enrichment Statistic' -weighted and 'Metric for Ranking Genes' -Signal2Noise. For unbiased hierarchical clustering of gene expression data, raw counts were converted to transcripts per million (TPM) then used as input in the HierarchicalClustering module in GenePattern[73] (Pearson correlation, average linkage). A detailed summary of these analyses can be found in Supplementary Table 2.

Analysis of public gene expression data and heatmap rendering. The gene expression heatmaps and gene expression graphs (Fig. 1e) show publicly available data from the Immunological Genome Project (ImmGen; mouse) and the Gene Expression Omnibus (GEO) (https://www.ncbi.nlm.nih.gov/geo/): GSE2350 (human tonsil B cell subsets) and GSE139833. To generate the heatmaps, gene expression values were standardized (z-scores) across samples (rows) and then with the scaled data for heatmap generation using the HeatMapViewer tool in the GenePattern server (genepattern.org).

Quantification and statistical analysis. GraphPad Prism Software (v.8.4.2) was used for all statistical analyses. Details for each statistical test are indicated in both the corresponding figure legends and Methods. Significance levels (P values) are also reported in each figure legend. For RNA-seq experiments, four independent mouse donors per genotype were used and correct sample clustering was confirmed using principal component analysis before differential expression analysis.

For in vivo experiments, sample size was determined using G*Power[74] (80% power, significance level alpha < 0.05 and standard deviation determined from previous studies on GC development) to detect differences of >20% between groups in cell percentages, cell numbers or marker expression levels, using two-tailed tests.

Reporting Summary. Further information on research design is available in the Nature Research Reporting Summary linked to this article.

Data availability
RNA-seq datasets were deposited in the GEO database under accession no. GSE148570 (reference series). Additional preprocessed data are provided in Supplementary Tables 1 and 2. Data from publicly available datasets were used for additional analyses, as specified in individual figure legends: GEO (https://www.ncbi.nlm.nih.gov/geo/) datasets and records GSE2350, GSE139833 (human tonsil B cell subsets); GSE68349 and GSE67494 (chromatin immunoprecipitation data for BCL6 and histone marks in human GC B cells); and the Immunological Genome Project (https://www.immgen.org) for mouse B cell subset gene expression data. Source data are provided with this paper.

References
58. Zhang, M. et al. The role of natural IgM in myocardial ischemia–reperfusion injury. *J. Mol. Cell. Cardiol.* **41**, 62–67 (2006).
59. Llaudo, I. et al. C5aR1 regulates migration of suppressive myeloid cells required for costimulatory blockade-induced murine allograft survival. *Am. J. Transpl.* **19**, 633–645 (2019).
60. Hovingh, E. S., van den Broek, B. & Jongerius, I. Hijacking complement regulatory proteins for bacterial immune evasion. *Front. Microbiol.* **7**, 2004 (2016).
61. Mashiko, D. et al. Generation of mutant mice by pronuclear injection of circular plasmid expressing Cas9 and single guided RNA. *Sci. Rep.* **3**, 3355 (2013).
62. Kwan, W. H. et al. Antigen-presenting cell-derived complement modulates graft-versus-host disease. *J. Clin. Invest.* **122**, 2234–2238 (2012).
63. Le, T. V., Kim, T. H. & Chaplin, D. D. Intraclonal competition inhibits the formation of high-affinity antibody-secreting cells. *J. Immunol.* **181**, 6027–6037 (2008).
64. Phan, R. T. & Dalla-Favera, R. The BCL6 proto-oncogene suppresses p53 expression in germinal-centre B cells. *Nature* **432**, 635–639 (2004).
65. Gitlin, A. D., Shulman, Z. & Nussenzweig, M. C. Clonal selection in the germinal centre by regulated proliferation and hypermutation. *Nature* **509**, 637–640 (2014).
66. Jacob, J. & Kelsoe, G. In situ studies of the primary immune response to (4-hydroxy-3-nitrophenyl)acetyl. II. A common clonal origin for periarteriolar lymphoid sheath-associated foci and germinal centers. *J. Exp. Med.* **176**, 679–687 (1992).
67. Lefranc, M. P. et al. IMGT, the international ImMunoGeneTics information system. *Nucleic Acids Res.* **37**, D1006–D1012 (2009).
68. Alamyar, E., Duroux, P., Lefranc, M. P. & Giudicelli, V. IMGT((R)) tools for the nucleotide analysis of immunoglobulin (IG) and T cell receptor (TR) V-(D)-J repertoires, polymorphisms, and IG mutations: IMGT/V-QUEST and IMGT/HighV-QUEST for NGS. *Methods Mol. Biol.* **882**, 569–604 (2012).
69. MacCarthy, T. et al. V-region mutation in vitro, in vivo, and in silico reveal the importance of the enzymatic properties of AID and the sequence environment. *Proc. Natl Acad. Sci. USA* **106**, 8629–8634 (2009).
70. Kim, D., Langmead, B. & Salzberg, S. L. HISAT: a fast spliced aligner with low memory requirements. *Nat. Methods* **12**, 357–360 (2015).
71. Liao, Y., Smyth, G. K. & Shi, W. featureCounts: an efficient general purpose program for assigning sequence reads to genomic features. *Bioinformatics* **30**, 923–930 (2014).
72. Love, M. I., Huber, W. & Anders, S. Moderated estimation of fold change and dispersion for RNA-seq data with DESeq2. *Genome Biol.* **15**, 550 (2014).
73. Reich, M. et al. GenePattern 2.0. *Nat. Genet.* **38**, 500–501 (2006).
74. Faul, F., Erdfelder, E., Lang, A. G. & Buchner, A. G*Power 3: a flexible statistical power analysis program for the social, behavioral, and biomedical sciences. *Behav. Res. Methods* **39**, 175–191 (2007).

Author contributions
A.C. contributed to the study design, performed the majority of in vivo and in vitro studies, prepared figures and wrote and edited the manuscript. D.H. and Z.H designed and prepared the DAF-TM targeting construct and performed in vitro characterization of the DAF-TM gene product in founder mice. Y.H and G.V. performed studies on DAF gene regulation by BCL6 experiments, BCR-seq and, together with M.P.R., performed RNA-seq analyses and reviewed and edited the manuscript. F.O. performed experiments, including all studies with B1-8hi mice, and reviewed and edited the manuscript. D.H. and S.A.L. outlined the strategy for DAF-TM generation, served as critical reviewers of data and edited the manuscript. D.D.-S. and P.S.H. conceptualized, designed and supervised the project, reviewed all data, wrote and edited the manuscript and provided funding.

Competing interests
The authors declare no competing interests.

Additional information
Extended data is available for this paper at https://doi.org/10.1038/s41590-021-00926-0.

Supplementary information The online version contains supplementary material available at https://doi.org/10.1038/s41590-021-00926-0.

Correspondence and requests for materials should be addressed to D.D.-S. or P.S.H.

Peer review information *Nature Immunology* thanks Anne Astier, Michael Carroll and the other, anonymous, reviewer(s) for their contribution to the peer review of this work. Peer reviewer reports are available. L. A. Dempsey was the primary editor on this article and managed its editorial process and peer review in collaboration with the rest of the editorial team.

Reprints and permissions information is available at www.nature.com/reprints.
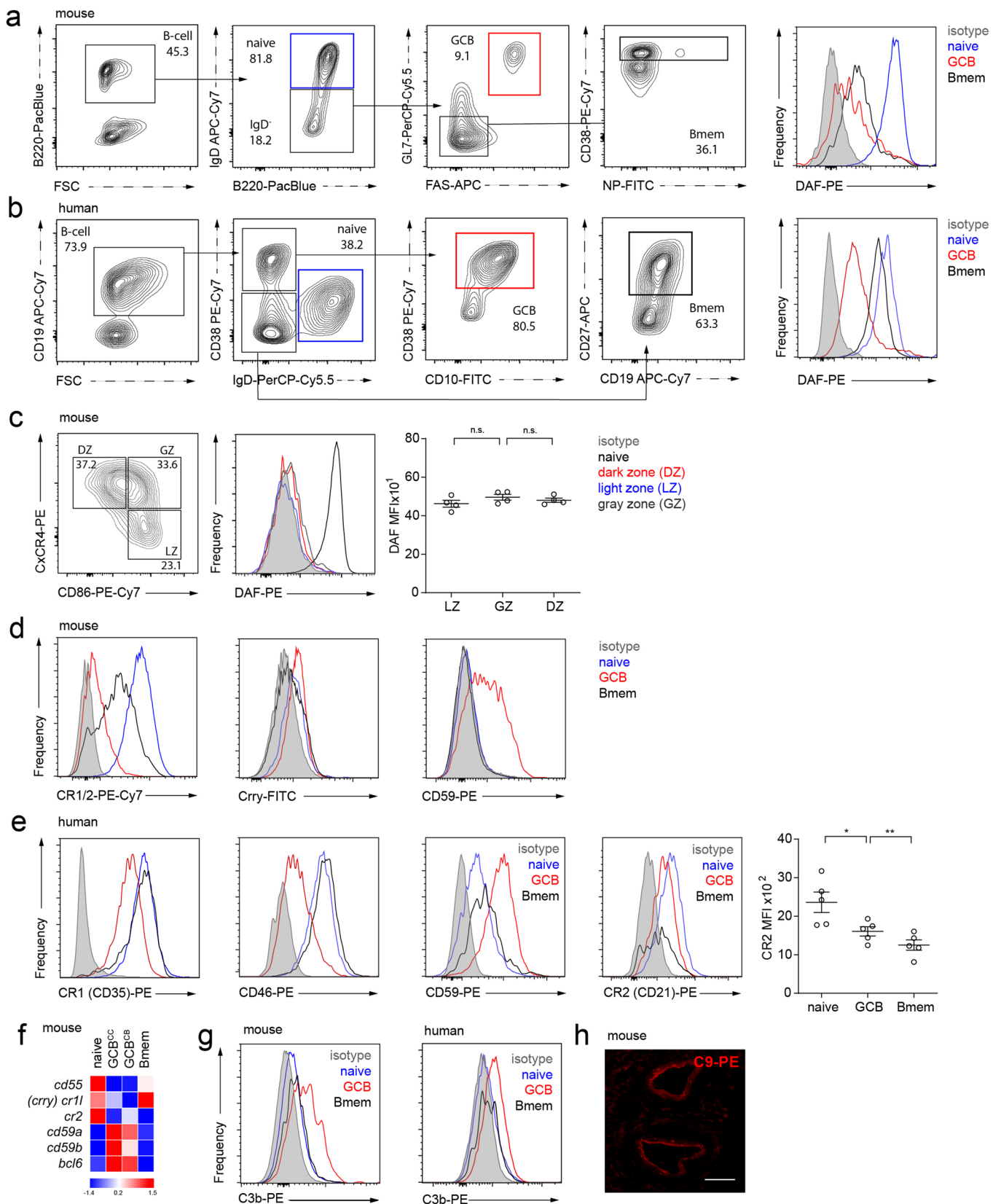
Extended Data Fig. 1 | See next page for caption.

Extended Data Fig. 1 | Distribution of complement regulator expression in mature B cell subsets. a,b, Gating strategy for flow cytometry analysis of murine (**a**) and human (**b**) naïve, GC and memory B cells, with representative histograms of DAF expression across B cell subsets. **c**, DAF expression on light (LZ), dark (DZ) and grey zone (GZ) GC B cells defined by CXCR4 and CD86 expression (left) with representative histograms (middle) and quantitation (right). **d**, Representative flow plots of mouse B cell subsets for CR1/2, Crry, and CD59 expression. **e**, Representative histograms of human tonsillar B cell subsets for CR1(CD35), CD46, CD59 and CR2(CD21) expression, with quantitation of CR2/CD21 expression (right panel). **f**, Heatmap, source: ImmGen database, with row-normalized mRNA expression of complement regulators and *Bcl6* in different murine B cell subsets. **g**, Representative histograms showing C3b staining on murine (left) and human (right) B cell subsets. **h**, Representative (3 individual experiments) image of human tonsil staining with anti-C9 showing positive staining of vascular endothelium (positive control for Fig. 1g), scale bar 50 µm. Data are presented as MFI +/− SEM, *p < 0.05, **p < 0.01, ***p < 0.001 by ANOVA with Bonferroni post-test (**c,e**). Each dot represents a biological replicate. n.s., not significant.
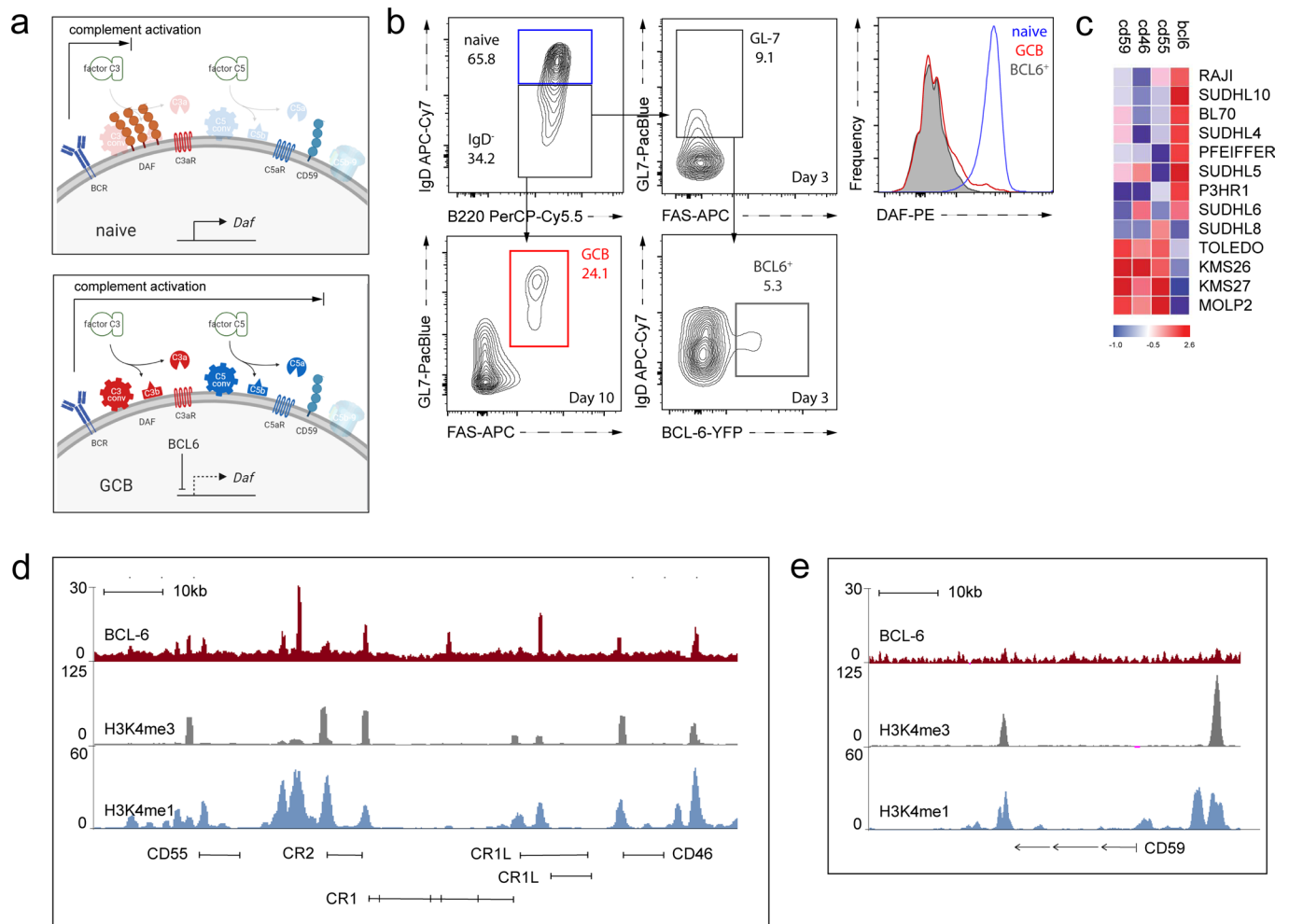
Extended Data Fig. 2 | BCL6 is inversely correlated with DAF expression and binds to regulatory regions of RCA genes. a, Schematic diagram illustrating effects of absent DAF with persistent CD59 expression on complement activation products on naïve (top) vs GC (bottom) B cells. **b**, Gating strategy for DAF/CD55 expression on immunized BCL6-YFP+ reporter mice, d3 post-immunization with SRBCs including d10 naïve and GC B cell controls (complementary to Fig. 2a). **c**, Heat map depicting relative mRNA expression levels (row-normalized) for BCL6 and complement regulators on human B cell lymphoma cell lines (Diffuse Large B cell lymphoma and selected Burkitt lymphoma cell lines: Raji, BL70, P3HR1; and Multiple Myeloma cell lines: KMS26, KMS27 and MOLP2). Data extracted from the Cancer Cell Line Encyclopedia (CCLE) repository[1,2]. **d-e**, Schematic depiction of ChIP-seq tracks for BCL6 and selected histone marks at the human RCA (**d**) and CD59 (**e**) gene loci. Data extracted from GEO records GSE68349, GSE67494[3,4].
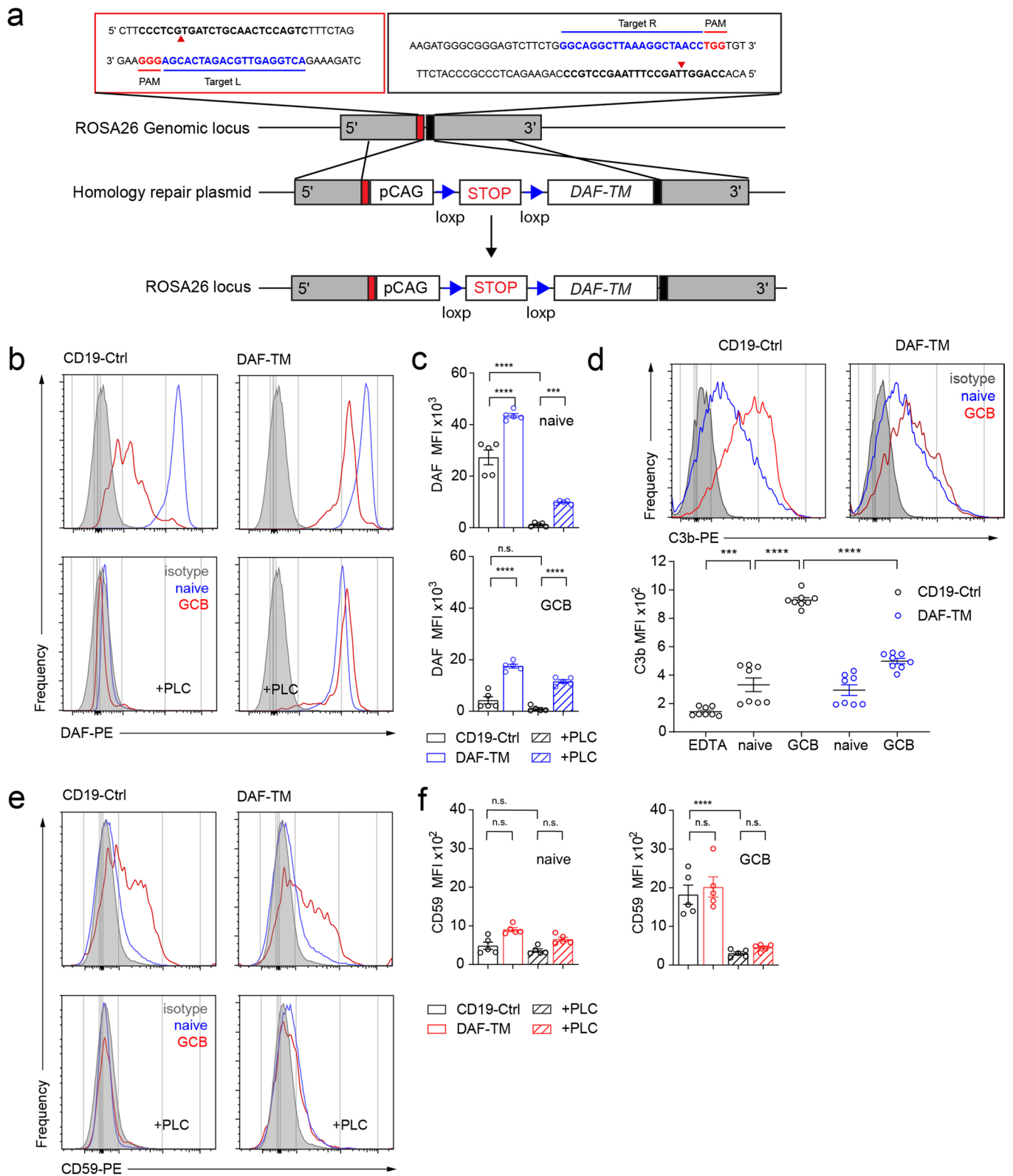
Extended Data Fig. 3 | See next page for caption.

Extended Data Fig. 3 | Design and validation of conditional DAF-TM transgenic mice. a, Schematic of Crispr/Cas9n strategy for producing DAF-TM transgenic mouse. The sequence inset shows a segment of the WT *Rosa26* locus and our targeting gRNA design. The PAM (Protospacer Adjacent Motif) is highlighted in red. The 5′–NGG–3′ sequence is the PAM consensus for binding of S. pyogenes Cas9 and Cas9D10A (Cas9n) nickase variant. The sequences in blue adjacent to the PAM sequences (Target L and Target R) indicate the target sites for Cas9n mediated cleavage. These sequences are identical with the spacer sequences in gRNA-A and gRNA-B, respectively. Cas9n nicks the target DNA at sites indicated with red triangles. Offset nicking induces recombination between the genomic *Rosa26* locus and the homology arms in the repair plasmid that results in insertion of the DAF-TM transgenic construct between the WT *Rosa26* segments indicated with red and black boxes. **b-c**, Representative flow cytometry plots (**b**) and quantified results (**c**) of DAF staining on naïve and GC B cells from DAF-TM[CD19] mice (DAF-TM x *CD19*-Cre^{+/-}) and CD19^{+/-} control mice in the absence or presence of phospholipase C (PLC), n = 5 independent biological replicates. Note that PLC totally removes native surface DAF from Control (*CD19*-Cre^{+/-}) B cells. In DAF-TM[CD19] B cells, PLC removed native (GPI-anchored) DAF leaving lower but detectable levels of transgenic DAF resistant to PLC cleavage. **d**, Representative histograms (top) and quantification (bottom) depicting lower C3b deposition on B cell subsets from DAF-TM[CD19] compared to control *CD19*-Cre^{+/-} mice. **e-f**, Representative flow cytometry plots (**e**) and quantified results (**f**) of CD59 staining on naïve and GC B cells from DAF-TM[CD19] (DAF-TM x *CD19*-Cre^{+/-}) and *CD19*-Cre^{+/-} control mice in the absence or presence of phospholipase C (PLC), n = 5 independent biological replicates. PLC removed the GPI-anchored CD59 from the surfaces of GC B cells in both *CD19*-Cre^{+/-} and DAF-TM[CD19] B cells.; All data are presented as MFI +/− SEM, *p < 0.05,**p < 0.01, ***p < 0.001, ****p < 0.0001 by one-way ANOVA with Bonferroni post-test (**c,d,f**). n.s., not significant. Each dot represents a biological replicate.
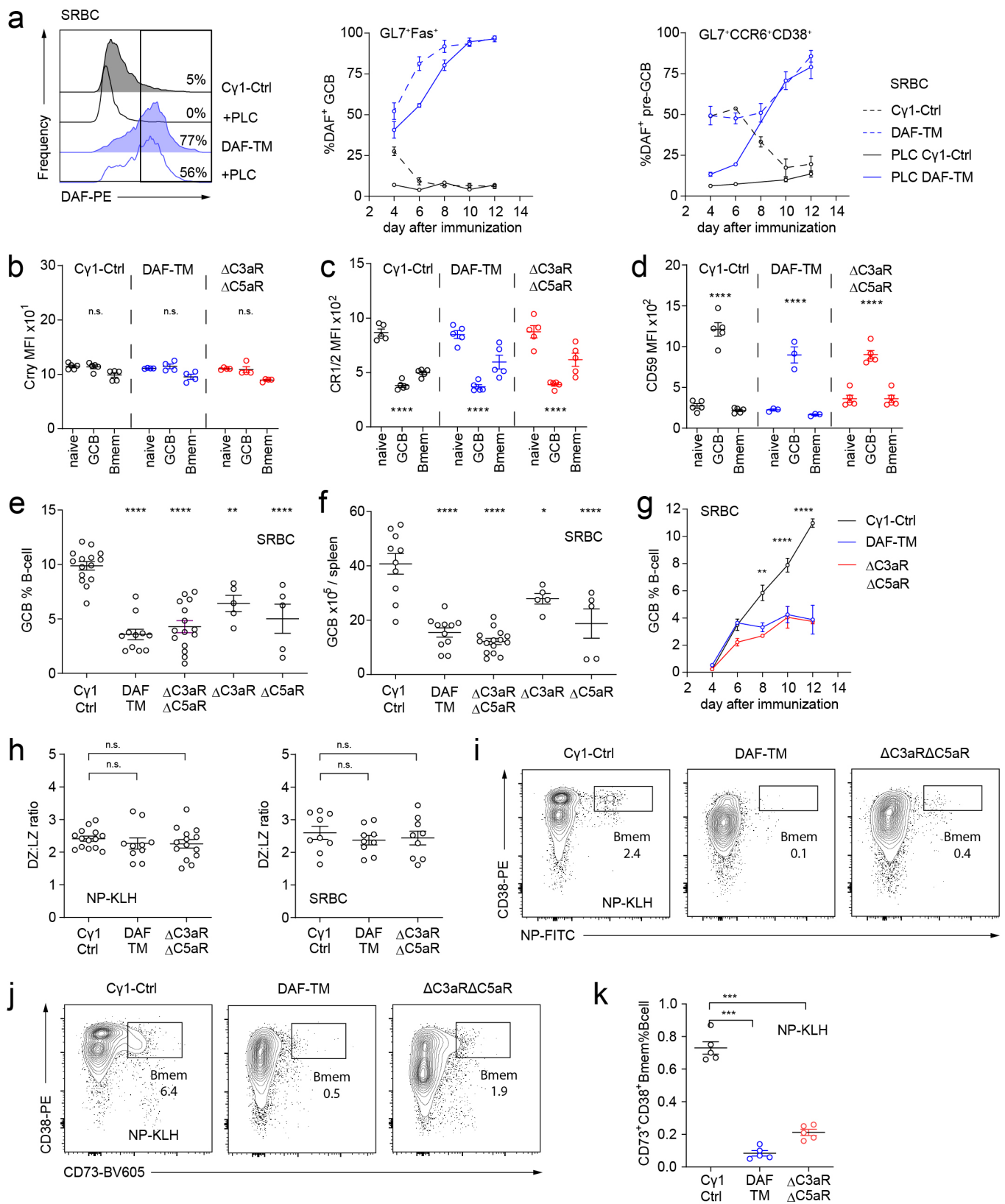
Extended Data Fig. 4 | See next page for caption.

Extended Data Fig. 4 | Extended characterization of GC and antibody responses in GC- (*Cγ1*-Cre) and B cell-specific (CD19-cre) DAF-TM and ΔC3aR1, ΔC5aR1 mice. a, representative histograms (left) and kinetics of total surface DAF and DAF-TM (PLC-resistant) expression on IgD⁻Fas⁺GL7⁺ GC B cells (middle) and IgD⁻GL7⁺CCR6⁺CD38⁺ B cells (right) in DAF-TM^{Cγ1} (DAF TM) and control *Cγ1*-Cre^{+/-} (Cγ1 Ctrl) mice. Note the progressive accumulation of DAF-TM⁺ B cells over time, following the kinetics of *Cγ1*-Cre-driven recombination[5]. **b-d**, Quantified surface expression of Crry (**b**) CR1/2 (**c**), and CD59 (**d**) proteins on B cell subsets from *Cγ1*-Cre^{+/-} control, DAF-TM^{Cγ1} and, Δ*C3ar1/C5ar1*^{Cγ1} mice. **e-f**, Relative % (**e**) and absolute frequencies (**f**) of splenic GC B cells in d12 SRBC-immunized DAF-TM^{Cγ1} (DAF TM), Δ*C3ar1/C5ar1*^{Cγ1} (ΔC3aRΔC5aR) *C3ar1*^{Cγ1} (ΔC3aR), Δ*C5ar1*^{Cγ1} (ΔC5aR), and control *Cγ1*-Cre^{+/-} (Cγ1 Ctrl) mice. **g**, Kinetics of relative GC B cells frequencies in SRBC immunized DAF-TM^{Cγ1}, Δ*C3ar1/C5ar1*^{Cγ1} and *Cγ1*-Cre^{+/-} mice. **h**, Ratios of DZ (CXCR4⁺CD86⁺) vs LZ (CXCR4⁻CD86⁺) GC B cells d10 post-immunization with NP-KLH (left) or SRBC (right). **i**, Representative flow cytometry plots for CD38⁺NP⁺ memory B cells (Bmem), within B220⁺IgD⁻GL7⁻Fas⁻ spleen cell populations of NP-KLH-immunized *Cγ1*-Cre^{+/-} control, DAF-TM^{Cγ1} and Δ*C3ar1/C5ar1*^{Cγ1} mice (d12 post-immunization) (see also Fig. 3f). **j-k**, Representative flow cytometry plots (**j**) and quantified results (**k**) for CD38⁺CD73⁺ Bmem gated on B220⁺IgD⁻GL7⁻Fas⁻ spleen cells in NP-KLH-immunized *Cγ1*-Cre^{+/-} control, DAF-TM^{Cγ1} and Δ*C3ar1/C5ar1*^{Cγ1} mice on d12. Data are presented as MFI (**b-d**) or mean (**a**, **e-h**, **k**) +/− SEM *p < 0.05, **p < 0.01, ***p < 0.001, ****p < 0.0001 by ANOVA with Bonferroni post-test (**a-h**, **k**), For kinetics in (**g**), 3 genotypes were compared at each time point. Each dot represents a biological replicate. n.s., not significant.
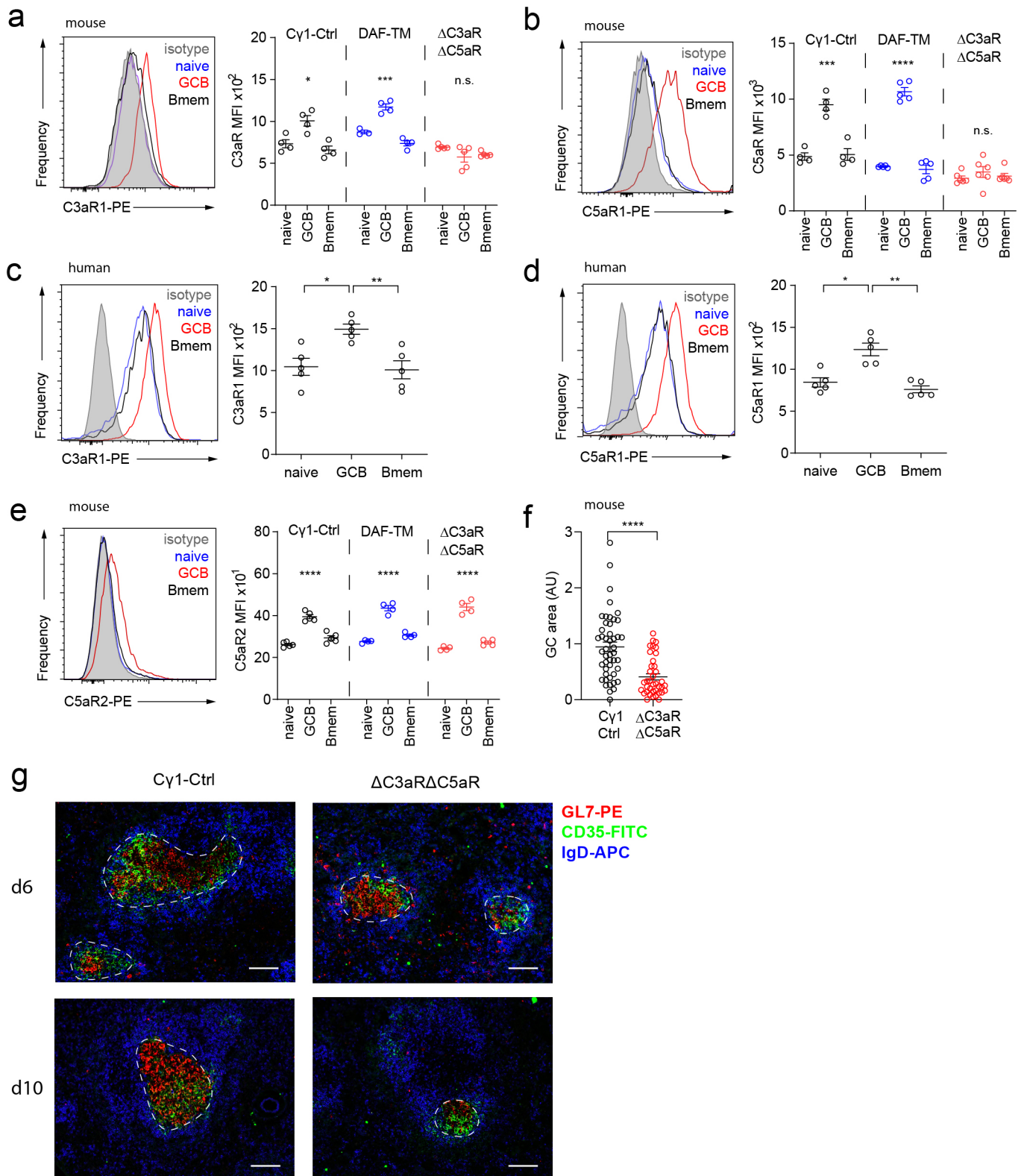
Extended Data Fig. 5 | See next page for caption.

Extended Data Fig. 5 | Analysis of C3aR1 and C5aR1 Expression in mouse and human B cell subsets. a-b, Representative histograms (left panels) and quantified results (right panels) for C3aR1 (**a**) or C5aR1 (**b**) expression on splenic B cell subsets of immunized control $C\gamma1$-Cre$^{+/-}$ mice. **c-d**, Representative histograms (left panels) and quantified results (right panels) for C3aR1 (**c**) and C5aR1 (**d**) expression on human tonsil B cell subsets. **e**, Representative histograms (left panels, $C\gamma1$-Cre$^{+/-}$ mice) and quantified results (right panel) for C5aR2 (C5L2) expression on B cell subsets from DAF-TM$^{C\gamma1}$ (DAF TM), $\Delta C3ar1/C5ar1^{C\gamma1}$ (ΔC3aRΔC5aR), and control $C\gamma1$-Cre$^{+/-}$ (Cγ1 Ctrl) mice on d10 after NP-KLH immunization. (**f**) Quantified GC sizes on d10 post-immunization and (**g**) representative IF images of GCs from d6 and d10 $\Delta C3ar1/C5ar1^{C\gamma1}$ and $C\gamma1$-Cre$^{+/-}$ mice post-SRBC immunization (spleen). Dotted lines in (**g**) outline GCs. Scale bar 50 μm. Data derived from 3 different tissue sections from each of 3 individual animals. Data are presented as MFI (**a-e**) or mean (**f**) ± SEM, *p < 0.05, **p < 0.01, ***p < 0.001 by ANOVA with Bonferroni post-test (**a-e**) or Students t-test (**f**). n.s., not significant. Each dot represents a biological replicate.
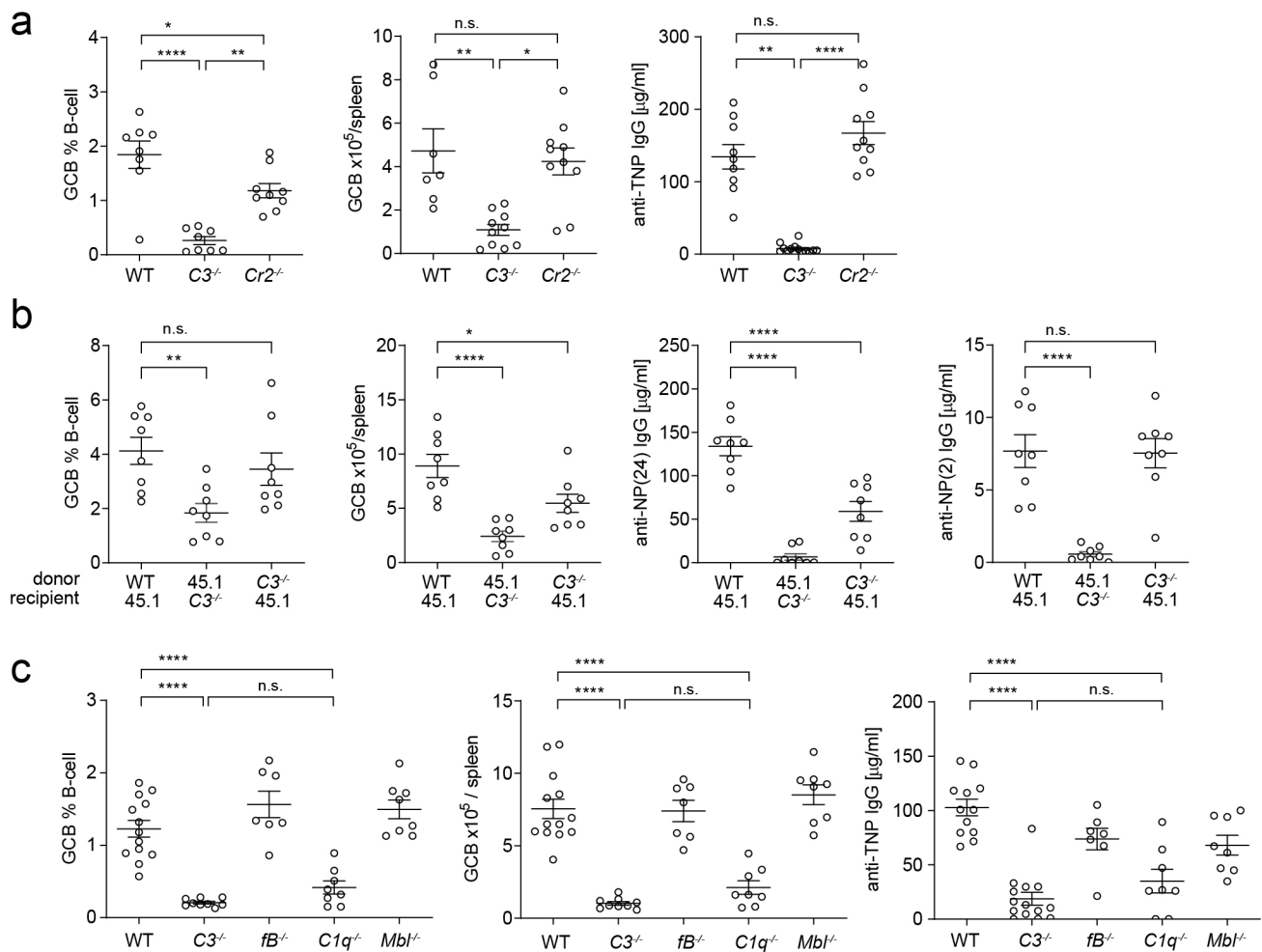
Extended Data Fig. 6 | Characterization of mouse GC and antibody responses in absence of CD21 or complement component expression. a, Relative (left), absolute frequency (middle) of GC B cells and serum anti-TNP antibodies (right panel) in groups of WT and germline, congenic, cohoused $C3^{-/-}$ and $Cr1^{-/-}$ ($Cr2^{-/-}$, CD21 null) mice on d14 after immunization with TNP-KLH (CR1 and CR2/CD21 derive from alternatively spliced transcripts from a single gene in mice). **b**, Quantified GC B cells (left 2 panels) and serum anti-NP antibodies (total, 3rd panel, high affinity 4th panel) in C3 BM chimeras and controls (see Methods). **c**, Relative (left), absolute frequency (middle) of GC B cells and serum anti-TNP antibodies (right panel) in groups of WT and germline congenic cohoused $C3^{-/-}$, $fB^{-/-}$, $C1q^{-/-}$ and $Mbl1^{-/-}Mbl2^{-/-}$ ($Mbl^{-/-}$) mice on d14 after immunization with TNP-KLH. Data are presented as mean ± SEM; *p < 0.05, **p < 0.01, ***p < 0.001, ****p < 0.0001, by ANOVA with Bonferroni post-test. n.s. not significant. Each dot represents a biological replicate.
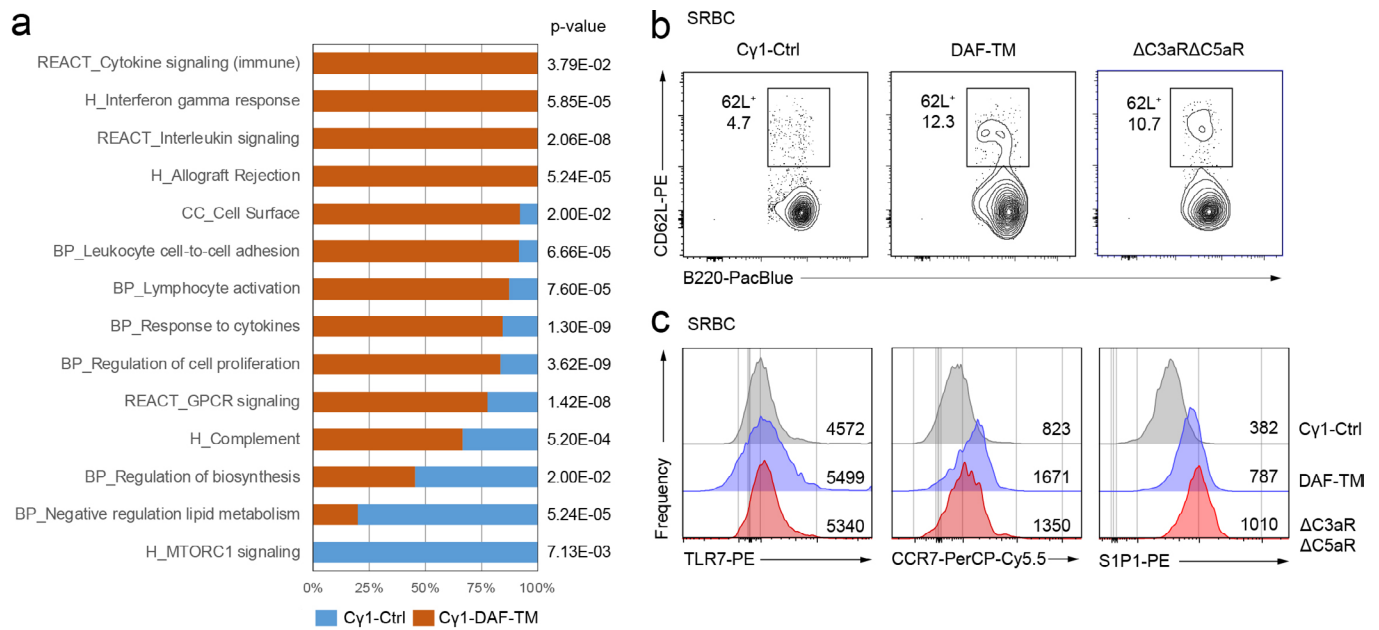
Extended Data Fig. 7 | Extended data for RNA-seq and surface marker signatures of GC B cells in DAF-TM$^{C\gamma1}$, ΔC3ar1/C5ar1$^{C\gamma1}$ and Cγ1-Cre$^{+/-}$ mice.
a, General summary of curated pathways up- or downregulated in RNA-seq gene expression datasets (relative enrichment) from DAF-TM$^{C\gamma1}$ (DAF TM) and control Cγ1-Cre$^{+/-}$ (Cγ1 Ctrl) mice (see also **Extended Data Table 2**). p-values hypergeometric distribution based on gene overlaps, with FDR q-value <0.05 (p-value after Benjamini and Hochberg correction for multiple hypothesis testing). **b**, Representative flow cytometry plots depicting the percentage of CD62L$^+$ GC B cells from DAF-TM$^{C\gamma1}$ (DAF TM), ΔC3ar1/C5ar1$^{C\gamma1}$ (ΔC3aRΔC5aR)· and control Cγ1-Cre$^{+/-}$ (Cγ1 Ctrl) mice on d10 after immunization with SRBC. **c**, Representative flow cytometry histograms for TLR7, CCR7 and S1P1 gated on IgD$^-$GL7$^+$Fas$^+$ GC B cells from DAF-TM$^{C\gamma1}$, ΔC3ar1/C5ar1$^{C\gamma1}$ and Cγ1-Cre$^{+/-}$ mice on d10 after immunization with SRBC (numbers correspond to MFI values).
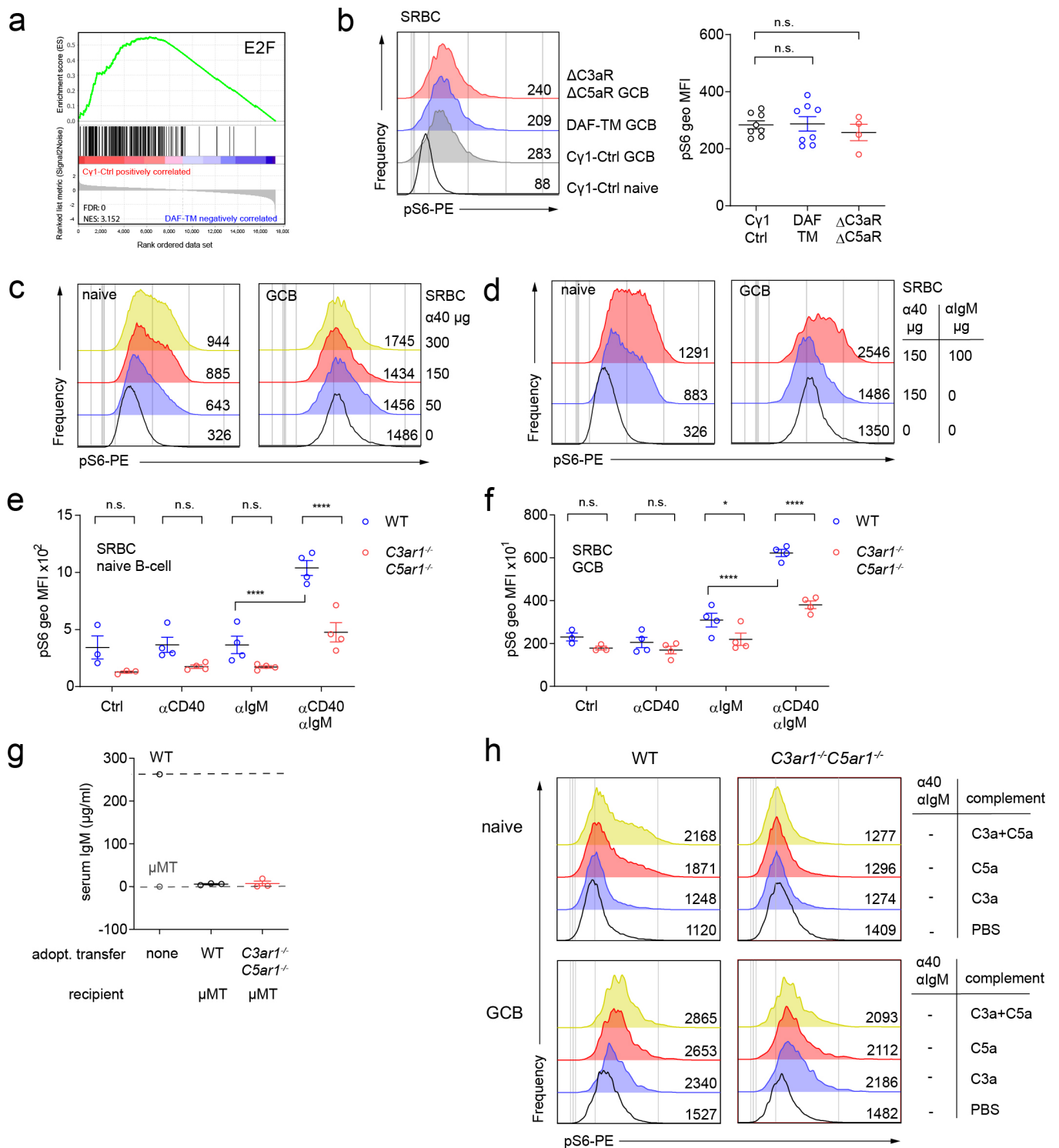
Extended Data Fig. 8 | See next page for caption.

Extended Data Fig. 8 | Extended data and experimental controls for RNA-seq analysis and mTOR signaling responses to CD40 and C3aR1/C5aR1 ligation. a, GSEA enrichment plot for E2F gene signature in DAF-TM^{Cg1} vs. $C\gamma1$-$Cre^{+/-}$ mice. NES, normalized enrichment score; FDR, false discovery rate (see also **Extended Data Table 2**). **b**, Representative histograms (left) and MFI (right) of pS6 levels in GC B cells (filled histograms) from DAF-TM$^{C\gamma1}$ (DAF TM), Δ$C3ar1/C5ar1^{C\gamma1}$ (ΔC3aRΔC5aR) and control $C\gamma1$-$Cre^{+/-}$ (Cγ1 Ctrl) at d10 post-SRBC immunization (without anti-CD40 or anti-IgM F(ab')$_2$ stimulation). **c-d**, Representative histograms for pS6 levels in naïve (left) or GC B cells (right) from DAF-TM$^{C\gamma1}$, Δ$C3ar1/C5ar1^{C\gamma1}$ and $C\gamma1$-$Cre^{+/-}$ mice on d10 after SRBC immunization and 4 h after i.v. anti-CD40 antibody at the indicated dose (**c**), or anti-CD40+ anti-IgM F(ab')$_2$ as indicated. **e-g**, 2×10^7 WT or C3aR1$^{-/-}$C5aR$^{-/-}$ B cells were transferred into µMT recipients, which were subsequently immunized with SRBC. Levels of pS6 were quantified in GC (**e**) or naïve B cells (**f**) d10 post-immunization and 4 h after i.v anti-CD40/anti-IgM F(ab')$_2$ stimulation **g**, ELISA for serum IgM in adoptive hosts (d10), including µMT negative and a WT B6 positive controls. **h**, Representative pS6 staining histograms of *in vitro* cultured naïve (top) and GC (bottom) B cells, stimulated for 20 min ± recombinant C3a, C5a (alone), without anti-CD40/ anti-IgM F(ab')$_2$ stimulation. n = 5/group, 2 independent experiments. Data are presented as MFI (**b**, **e-f**) or mean (**g**) +/- SEM, *p < 0.05, **p < 0.01, ***p < 0.001, ****p < 0.0001, by ANOVA with Bonferroni post-test (**b, e-f**). n.s, not significant. Each dot represents a biological replicate.

Corresponding author(s):   Peter S. Heeger & David Dominguez-Sola

Last updated by author(s):   Jan 26, 2021

Reporting Summary

Nature Research wishes to improve the reproducibility of the work that we publish. This form provides structure for consistency and transparency in reporting. For further information on Nature Research policies, see our Editorial Policies and the Editorial Policy Checklist.

Statistics

For all statistical analyses, confirm that the following items are present in the figure legend, table legend, main text, or Methods section.

n/a	Confirmed	
☐	☒	The exact sample size (*n*) for each experimental group/condition, given as a discrete number and unit of measurement
☐	☒	A statement on whether measurements were taken from distinct samples or whether the same sample was measured repeatedly
☐	☒	The statistical test(s) used AND whether they are one- or two-sided *Only common tests should be described solely by name; describe more complex techniques in the Methods section.*
☐	☒	A description of all covariates tested
☐	☒	A description of any assumptions or corrections, such as tests of normality and adjustment for multiple comparisons
☐	☒	A full description of the statistical parameters including central tendency (e.g. means) or other basic estimates (e.g. regression coefficient) AND variation (e.g. standard deviation) or associated estimates of uncertainty (e.g. confidence intervals)
☐	☒	For null hypothesis testing, the test statistic (e.g. *F*, *t*, *r*) with confidence intervals, effect sizes, degrees of freedom and *P* value noted *Give P values as exact values whenever suitable.*
☒	☐	For Bayesian analysis, information on the choice of priors and Markov chain Monte Carlo settings
☒	☐	For hierarchical and complex designs, identification of the appropriate level for tests and full reporting of outcomes
☒	☐	Estimates of effect sizes (e.g. Cohen's *d*, Pearson's *r*), indicating how they were calculated

Our web collection on statistics for biologists contains articles on many of the points above.

Software and code

Policy information about availability of computer code

Data collection	FACS Diva software v 8.0 (BD Biosciences) used for flow cytometry data collection
Data analysis	Prism 8.4.2 software (Graphpad) (for all statistical analyses) FlowJo 10.6.2 (BD) Illustrator CS5 (Adobe Systems Inc) Adobe Photoshop CS6 V13.0 (Adobe Systems Inc) Biorender, available at BioRender.com GenePattern suite, Broad Institute (genepattern.org) HISAT2, ver 2.1.0, available at http://daehwankimlab.github.io/hisat2/ featureCounts tool, from Subread package at http://subread.sourceforge.net DESeq2 tool ver 1.10.1, available at GenePattern.org Gene Set Enrichment Analysis (GSEA) ver 4.0.3 (Broad Institute at https://www.gsea-msigdb.org/gsea/index.jsp) NIS Elements software, ver 4.20 (Nikon)

For manuscripts utilizing custom algorithms or software that are central to the research but not yet described in published literature, software must be made available to editors and reviewers. We strongly encourage code deposition in a community repository (e.g. GitHub). See the Nature Research guidelines for submitting code & software for further information.

Data

All manuscripts must include a data availability statement. This statement should provide the following information, where applicable:

- Accession codes, unique identifiers, or web links for publicly available datasets
- A list of figures that have associated raw data
- A description of any restrictions on data availability

> All RNA-Seq datasets were deposited in the Gene Expression Omnibus (GEO) database, under accession number GSE148570 (reference series). Additional preprocessed data provided in Supplementary tables 1 and 2.
> Data from publicly available datasets was used for additional analyses (specified in the figure legends):
> Gene Expression Omnibus (https://www.ncbi.nlm.nih.gov/geo/) datasets, records GSE2350, GSE139833 (human tonsil B cell subsets); GSE68349 and GSE67494 (chromatin immunoprecipitation data for BCL-6 and histone marks in human GC B cells).
> Immunological Genome Project (ImmGen; https://www.immgen.org) for mouse B cell subset gene expression data.

Field-specific reporting

Please select the one below that is the best fit for your research. If you are not sure, read the appropriate sections before making your selection.

☒ Life sciences   ☐ Behavioural & social sciences   ☐ Ecological, evolutionary & environmental sciences

For a reference copy of the document with all sections, see nature.com/documents/nr-reporting-summary-flat.pdf

Life sciences study design

All studies must disclose on these points even when the disclosure is negative.

Sample size	Sample size estimated using G*Power61 (80% Power, significance level -alpha <0.05 and standard deviation determined from previous studies on GC development), to detect differences >20% between groups in cell percentages, cell numbers or marker expression levels using two-tailed tests.
Data exclusions	No data excluded from analyses
Replication	Each figure panel represents at least 3 independent experiments with multiple biological replicates (single mice or tissues samples, n>3) and 3-5 technical replicates. For in vitro experiments with lymphoma cell lines (Fig 3), each experimental replicate represents a new (fresh) culture of cryopreserved cells from different passages post-antibiotic selection. For RNA-Seq experiments, we used 4 independent mice donors per genotype and confirmed correct sample clustering using Principal Component Analysis prior to differential expression analysis.
Randomization	Given the nature of the comparisons (genetic models), we did not randomize mice into experimental groups or blind the investigators to group allocation. To control for potential co-variates, all animal experiments used age- (6-12 weeks) and sex-matched animals from the same litters or if necessary (C57Bl/6 control animals) mice were maintained in the same room and co-housed within the same cages for >2 weeks, to limit potential effects of microbiome differences.
Blinding	Given the nature of the comparisons (genetic models), we did not randomize mice into experimental groups or blind the investigators to group allocation. Blinding was done only during data collection by using number identifiers instead of genotypes, and sample identity (genoptype) retrieved later during data analysis (data analysis parameters were pre-established and universal for all samples)

Reporting for specific materials, systems and methods

We require information from authors about some types of materials, experimental systems and methods used in many studies. Here, indicate whether each material, system or method listed is relevant to your study. If you are not sure if a list item applies to your research, read the appropriate section before selecting a response.

Materials & experimental systems

n/a	Involved in the study
☐	☒ Antibodies
☐	☒ Eukaryotic cell lines
☒	☐ Palaeontology and archaeology
☐	☒ Animals and other organisms
☒	☐ Human research participants
☒	☐ Clinical data
☒	☐ Dual use research of concern

Methods

n/a	Involved in the study
☒	☐ ChIP-seq
☐	☒ Flow cytometry
☒	☐ MRI-based neuroimaging

Antibodies

Antibodies used

ANTI-MOUSE ANTIBODIES
anti-B220 PacBlue (clone RA3-6B2) BD 560472
anti-C3aR (clone 14D4) Hycult HM1123
anti-C3b (clone 2/11) Hycult (IF) HM1065
anti-C3b PE (clone 10C7) Cederlane CL7632PE
anti-C5aR PE (clone 20/70) Biolegend 135806
anti-Caspase 3 PE (clone C92-605) BD 561011
anti-CCR6 PE-Cy7 (clone 29-2L17) Biolegend 129816
anti-CCR7 PerCP-Cy5.5 (clone 4B12) Biolegend 120116
anti-CD38 PE-Cy7 (clone 90) eBioscience 25-0381-82
anti-CD40 (clone FGK4.5/FGK45) BioXcell BP0016-2
anti-CD40 PE (clone 3/23) BD 553791
anti-CD45.1 PE (clone A20) BD 12-0453-82
anti-CD45.1 Brilliant Violet 605TM (clone A20) Biolegend 110738
anti-CD45.2 FITC (clone 104) BD 553772
anti-CD59 PE (clone mCD59.3) Biolegend 143103
anti-CD62L PE (clone MEL-4) Tonbo bioscience 50-0621-U-200
anti-CD73 PE-Cy7 (clone TY/11.8) Biolegend 127223
anti-CD86 PE-Cy7 (clone GL-1) Biolegend 105014
anti-Crry FITC (clone 512) ThermoFischer MA5-17553
anti-CR1/2 PE-Cy7 (clone 7E9) Biolegend 123419
anti-CxCR4 PE (clone 2B11) eBioscience 12-9991-82
anti-DAF/CD55 PE (clone RIKO5) BD (IF) 558037
anti-DAF/CD55 APC (clone RIKO3) Biolegend 131806
anti-FAS (CD95) APC (clone Jo2) BD 563647
anti-FAS (CD95) Alexa Fluor® 647 (clone Jo2) BD 563647
anti-GL-7 FITC (clone GL7) BD (IF) 553666
anti-GL-7 PerCP/Cyanine5.5 Biolegend 144609
anti-IgD APC (clone 11-26c) eBioscience (IF) 4323188
anti-IgD APC-Cy7 (clone 11-26c) eBioscience 47-5993-82
anti-IgD biotin (clone 11-26c.2a) Biolegend 405734
anti-IgD Brilliant Violet 711TM (clone 11-26c.2a) Biolegend 405731
anti-IgG2a (clone 2A3) BioXcell BP0089
anti-Ki-67 PE (clone SolA15) eBioscience 12-5698-82
anti-λ PE (clone 407308) Biolegend 407308
anti-IgM (clone AB_2338450) Jackson Lab 115-005-020
anti-mouse IgG-HRP Southern Biotech 1036-05
anti-myc PE (clone D84C12) Cell Signaling 14819S
anti-pS6 PE (clone cupk43k) eBioscience 129007-42
anti-S1P1/EDG-1 (clone 713412) R&D MAB7089
anti-TNP (clone 107.3) BD 554054
anti-TLR7 PE (clone A9B10) BD 565557
Yellow fluorescent reactive dye Thermo Fischer L34967A

ANTI-HUMAN ANTIBODIES
Anti-Actin B (b-Actin) (clone AC-15) Sigma-Aldrich (WB) A5441-100UL
anti-BCL6 PE-Cy7 (clone &D1) BioLegend 358512
anti-BCL6 (clone H12) Santa-Cruz (WB) Sc-365618
anti-C3aR biotin (clone hC3aRZ8) BD 561178
anti-C3b PE (clone 3E7/C3b) Biolegend 846104
anti-C4d (clone 12D11) Hycult (IF) HM2229-20UG
anti-C5aR PE (clone S5/1) Biolegend 344303
anti-C5b (clone 568) Hycult (IF) HM2080-20UG
anti-C6 (clone WU 6-4) Hycult (IF) HM2276-20UG
anti-C9 (clone aE11) Hycult (IF) HM2167-20UG
anti-CCR6 BV421 (clone 11A9) BD 562515
anti-CD10 FITC (cloneHI10a) BD 340925
anti-CD19 APC-Cy7 (clone HIB19) Biolegend 302218
anti-CD21 PE (clone HB5) eBioscience 11-0219-42
anti-CD27 APC (clone O323) Biolegend 302810
anti-CD35 PE (clone E11) Biolegend 333406
anti-CD38 PE-Cy7 (clone LS198-4-3) Beckman Coulter A54189
anti-CD46 PE (clone E4.3) BD 564252
anti-CD59 PE (clone p282-H19) BD 560953
anti-DAF/CD55 PE (clone 67 (N-L063) Thermo Fischer MHCD5504
anti-DAF/CD55 PE (clone IA10) BD 561901
anti-IgD PerCP-Cy5 (clone IA6-2) BD 561315

Validation

All commercial antibodies used in this study are routinely tested y the respective manufacturer. Related technical datasheets can be downloaded from the manufacturer's website using the catalog numbers provided above

Eukaryotic cell lines

Policy information about cell lines

Cell line source(s)	The human myeloma cell line KMS-27 was purchased from the Japanese Collection of Research Bioresources Cell Bank (Tokyo Japan, https://cellbank.nibiohn.go.jp/english/. The human diffuse large B-cell lymphoma (DLBCL) cell lines SU-DHL-5, SU-DHL-6, SU-DHL-10, OCI-LY7 and TOLEDO; and the Burkitt lymphoma cell line P3HR1 were kind gifts of Laura Pasqualucci (Columbia University Medical Center, New York, NY, USA). The genetic identity of these cell lines had been previously defined. DLBCL and BL cell lines were originally purchased from the DSMZ-German Collection of Microorganisms and Cell Cultures GmbH (www.dsmz.de) (SU-DHL-5, SU-DHL-6, SU-DHL-10 and OCI-Ly7) or ATCC (American Type Culture Collection), for P3KR1 and TOLEDO (www.atcc.org).
Authentication	We re-confirmed all cell line identities by multiplex cell authentication (Genetica Cell Line Testing).
Mycoplasma contamination	All cell lines tested negative in repeated analyses
Commonly misidentified lines (See ICLAC register)	No commonly misidentified cell lines were used in this study

Animals and other organisms

Policy information about studies involving animals; ARRIVE guidelines recommended for reporting animal research

Laboratory animals	All mice used in this study were matched by age (6-12 weeks) and sex, with equal distribution of males and females among genotypes. Mouse lines/strains used in this study, purchase from Jackson Laboratory (JAX): C57BL/6/J (B6, # 000664) B6;129S4-C3tm1Crr/J (C3tm1Crr, C3–/–, # 029661) B6.129P2(C)-Cd19tm1(cre)Cgn/J (# 6785, CD19-Cre+/–) C.129P2(Cg)-Ighg1tm1(cre)Cgn/J (# 010611, Cg1-Cre+/–) B6.SJL-Ptprca Pepcb/BoyJ (# 002014, CD45.1) B6.129S2-Ighmtm1Cgn/J (# 002288, muMT) Experiments using CD19-Cre+/– and Cg1-Cre+/– knock-in models were performed using Cre+/- heterozygotes. Germline B6 C3ar1–/–C5ar1–/– mice were generated as described in previous studies. Additional lines B6.129S4-Mbl1tm1Kata Mbl2tm1Kata/J (mbl1–/–mbl2–/–) from G. Stahl (Harvard Medical School, Boston MA) Complement factor B–/– (fB) originally produced by M. Pekna (Gothenburg, Sweden), gift from M. Zhang (SUNY Downstate, Brooklyn NY) CD21–/– originally produced by M Carroll (Harvard Medical School)69 (SUNY Downstate) B6(Cg)-C1qatm1d(EUCOMM)Wtsi/TennJ (Jax cat# 031675, C1q–/–) from B. Diamond (Feinstein Institute, Northwell Health, NY) Bcl-6YFPmice25 originally generated by T. Okada (Kyoto University, Kyoto, Japan), gift from S.Reiner, (Columbia University, New York, USA) B18hi BCR transgenic mice from M. Nussenzweig (Rockefeller University, NY, NY). B6 C5ar1fl/fl mice were described previously. B6 C3ar1fl/fl mice were generated from ES cells purchased from the EUCOMM consortium (see methods). These animals were crossed to B6.129S4-Gt(ROSA)26Sortm2(FLP*)Sor/J mice (JAX # 012930) to remove the neo cassette. C5ar1fl/fl and the C3ar1fl/fl animals were crossed to Cg1-Cre transgenics. Adjusted to ARRIVE guidelines.
Wild animals	No wild animals were used in this study
Field-collected samples	No field collected samples were used in this study
Ethics oversight	All animal protocols approved by the Center for Comparative Medicine and Surgery at the Icahn School of Medicine at Mount Sinai under Institutional Animal Care in accordance with guidelines of the Association for Assessment and Accreditation of Laboratory Animal Care International approval IACUC-2018-0014.

Note that full information on the approval of the study protocol must also be provided in the manuscript.

Flow Cytometry

Plots

Confirm that:

☒ The axis labels state the marker and fluorochrome used (e.g. CD4-FITC).

☒ The axis scales are clearly visible. Include numbers along axes only for bottom left plot of group (a 'group' is an analysis of identical markers).

☒ All plots are contour plots with outliers or pseudocolor plots.

☒ A numerical value for number of cells or percentage (with statistics) is provided.

Methodology

Sample preparation	We filtered mouse spleens (70um filters) lysed RBCs (ACK buffer, Lonza, Morristown NJ), and re-filtered them through 40-micron filters in PBS 1%FCS to produce single cell suspensions. For primary murine and human cells, we performed surface and intracellular staining using antibodies listed in Supplementary Table S3. For cell lines, we stained surface markers and then fixed and permeabilized in FoxP3 staining buffer (ThermoFisher Scientific/eBioscience) prior to intracellular staining.
Instrument	We analyzed samples on FACS Calibur, FACS LyricTM, FACS CantoTM II or Fortessa LSRII cytometers (BD Biosciences, San Jose CA) and CellQuest (FACS CAlibur) or FACS Diva software.
Software	We analyzed all flow cytometry results using FlowJo v10.6.1 software (FlowJo LLC, Ashland OR), version 10.
Cell population abundance	For germinal center B cells, average percentage was ~3% within the B cell fraction. Purity was above 98% for sorted GC populations.
Gating strategy	Germinal center (mouse): B220hi>IgDlo>FashiGL7hi PreGC (mouse): B220hi>IgDlo>GL7hi>Bcl6 hi vs CCR6hi Germinal center (human): CD19hi>IgDlo>CD38hiCD10hi Naive B (mouse): B220hi, IgDhi Naive B (human):CD19hi, IgDhi Memory B (mouse):B220hi>IgDlo>FasloGL7lo>CD38hi>NP+(IgG1+), CD73+/- Memory B (human): CD19hi>IgDlo>CD38lo>CD27hi Light zone/dark zone (GC gate): LZ (CD83hi, CXCR4lo); DZ (CD83lo, CXCR4hi) See Extended Data for additional information.

☒ Tick this box to confirm that a figure exemplifying the gating strategy is provided in the Supplementary Information.